Energy Conversion and Management 365 (2026) 121768

Contents lists available at ScienceDirect

Energy Conversion and Management

journal homepage: www.elsevier.com/locate/enconman

Operational dynamics and long-term stability in the novel CO_2-based electrothermal energy and geological storage system in salt cavities[☆]

A. Carro[a,b,*], J. Carneiro[c,d], S. Unger[f], D. Behnous[d,e], S. Fogel[f], R. Chacartegui[a,g]

[a] Dpto. Ingeniería Energética. Universidad de Sevilla, Camino de los Descubrimientos s/n, 41092 Sevilla, Spain
[b] Departamento de Ingeniería, Universidad Loyola Andalucía, Av. de las Universidades, 2, Dos Hermanas, 41704 Sevilla, Spain
[c] CREATE/IIFA, Geosciences Department, Universidade de Évora, R. Romão Ramalho 59, 7000-671 Évora, Portugal
[d] Converge!. Lda, Parque de Ciência e Tecnologia do Alentejo, R. Luís Adelino da Fonseca, Lt 1ª, 7005-841 Évora, Portugal
[e] Laboratory of Physical Engineering of Hydrocarbons, Faculty of Hydrocarbons and Chemistry, University M'Hamed Bougara of Boumerdes (UMBB), 35000 Boumerdes, Algeria
[f] Helmholtz-Zentrum Dresden-Rossendorf, Institute of Fluid Dynamics, Bautzner Landstr. 400, 01328 Dresden, Germany
[g] Universidad de Sevilla, Laboratory of Engineering for Energy and Environmental Sustainability, 41092 Seville, Spain

ARTICLE INFO

Keywords:
Thermal energy storage
Carnot battery
Transcritical CO_2
Geological storage
Salt cavities

ABSTRACT

The massive integration of renewable energy sources and the development of advanced technologies to mitigate climate change are key factors in the energy transition towards a sustainable model. Increasing the contribution of renewables to the electricity market requires developing new energy storage systems. The novel CO_2-based electrothermal energy and geological storage system could be a viable option for large-scale storage in renewable power generation plants in the near future. This system utilises transcritical CO_2 cycles to convert electrical energy into thermal and mechanical energy, enabling integration with carbon capture and storage systems in geological formations, with an initial efficiency range of 52.8–61.5%. This dual approach enhances energy storage capabilities and contributes to reducing atmospheric CO_2 levels, offering a sustainable solution to address both energy and environmental challenges. This study evaluates, for the first time, the subsurface potential as a thermohydraulic buffer that ensures long-term operational stability and pressure management. Through long-term temporal simulations, a numerical model featuring coupled thermohydraulic simulations has been developed to incorporate subsurface heat transfer processes, considering a salt cavern scenario. Different scenarios are analysed depending on the characteristics of the production/injection processes, well depth, cavern size, or storage time. The research identifies a critical transition from an initial transient phase to a dynamic steady state. The results demonstrate that while operational fluid streams almost entirely govern the system's short-term energetic response, geothermal interaction could be critical for long-term stabilisation. The energy gain during injection directly influences the required CO_2 conditions at the wellhead. Wellhead pressure and temperature must be adjusted according to the desired conditions at the bottomhole. Maintaining high-pressure conditions in the salt cavern is essential to ensure proper coupling with the surface cycles and to operate with high electricity-to-electricity conversion efficiencies, reaching the range of 50.3–65.6% when the pressure approaches the upper limit. Active management of mass flow rates and pressures, along with advanced thermal control strategies, will be essential to improve system efficiency and flexibility.

1. Introduction

In recent decades, the transition toward a more sustainable energy model has driven an unprecedented expansion of renewable energy sources, such as solar photovoltaic (PV) and wind power [1]. However, the growing penetration of these technologies has highlighted one of their main limitations: their intermittent nature and dependence on weather conditions. This variability introduces significant challenges to the stability and reliability of electricity grids, making it difficult to balance energy supply and demand consistently [2]. Given this scenario, the need to develop efficient, flexible, and scalable energy storage systems has become a priority to guarantee the security of the electricity supply and facilitate the massive integration of renewables into the

☆ This article is part of a special issue entitled: 'SDEWES 2025 - ECM' published in Energy Conversion and Management.

* Corresponding author at: Dpto. Ingeniería Energética. Universidad de Sevilla, Camino de los Descubrimientos s/n, 41092 Sevilla, Spain.
E-mail address: andrescarro@us.es (A. Carro).

https://doi.org/10.1016/j.enconman.2026.121768

Available online 11 June 2026

Nomenclature

CCS	Carbon Capture and Storage
CEEGS	CO_2-based Electrothermal Energy and Geological Storage
CO_2	Carbon dioxide
HE	Heat Engine
HP	Heat Pump
HT	High temperature
hx	Heat exchanger
LCOS	Levelised cost of storage
LDES	Long-Duration Energy Storage
LT	Low temperature
ORC	Organic Rankine Cycle
PCHE	Printed circuit heat exchangers
PTES	Pumped Thermal Energy Storage
PV	Photovoltaic
RTE	Round-trip Efficiency
sCO_2	Supercritical CO_2
tCO_2	Transcritical CO_2
TES	Thermal Energy Storage
TRL	Technology Readiness Level

global energy mix [3] and decarbonisation of energy-using sectors, essential for tackling climate change [4]. Currently, the main large-scale electricity storage technologies include reversible pumped hydro and compressed air storage [5]. While they have demonstrated operational effectiveness, these solutions face significant limitations related to geographic availability, high infrastructure costs, and environmental restrictions [6]. The global transition toward a decarbonized energy grid necessitates the deployment of Long-Duration Energy Storage (LDES) to manage the inherent intermittency of renewable sources. In response to these challenges, thermal energy storage (TES) systems are emerging as a robust and versatile alternative, allowing the storage of surplus electrical energy in the form of thermal energy, or heat, which can be retained for long periods and subsequently used for power generation or industrial thermal processes [7]. Their high storage capacity, low relative cost, and compatibility with diverse energy sources position TES as a strategic option in the development of more flexible and sustainable energy grids [8].

Among emerging thermal–mechanical candidates, Carnot Batteries, also known as Pumped Thermal Energy Storage (PTES), have gained significant attention due to their high energy density and lack of geographical constraints [9]. This concept is based on converting surplus electricity into heat using heat pumps, storing that heat in high-thermal-capacity materials, and subsequently converting it back into electricity using heat engines, such as steam turbines or Brayton cycles [10]. Its name refers to the Carnot cycle, as its overall efficiency is strongly influenced by the temperature difference between the cycle's sources or thermal storage [9]. It is still in the development and pilot implementation phase, but it offers key advantages, such as the use of mature technologies, low storage material costs, a long service life, and potential for integration with existing thermal infrastructure [11]. Carnot battery systems have been studied by many researchers, addressing various aspects of the cycle. The review on Carnot batteries of Vecchi et al. [12] shows the differences in the techno-economics of various Carnot Battery technologies, the wide range of some performance metrics and a certain discrepancy between the systems addressed by the scientific community and the projects under development. The relevant technical aspects of the thermal storage were studied in [13]. The state-of-the-art of the thermal storage system is presented and classified. It was found that solid and sensible TES units can be represented as an efficient component of a Carnot Battery in the high temperature range. A more general analysis of TES technologies for achieving carbon neutrality was done by Zhao et al. [14], investigating both TES and Carnot batteries. The advantages and challenges of different heat storage technologies and of Carnot batteries for carbon-neutrality processes were analysed. Furthermore, several authors address the optimisation of Carnot batteries to enhance round-trip efficiency or reduce system cost. Hence, the influence of standard engineering parameters such as heat source conditions and module efficiency on the overall performance of the system was studied in [15]. The results show that changes in compressor efficiency have little effect on energy storage cost ($<$5%) compared with changes in turbine efficiency. A multi-objective algorithm is used to identify the optimal design parameters, yielding an optimal solution with an efficiency of 48.95% and a levelized cost of storage (LCOS) of 0.319 $\$\cdot kWh^{-1}$. Wang et al. analysed the heat transfer fluid and several other parameters of a Carnot battery. [16]. A multi-criteria decision-making method was employed to determine the optimal system configurations and working fluids for different decision criteria. When economic considerations dominate, a system with helium as the working fluid is preferred. Three cities in China were studied as potential application sites for investigating the feasibility of a Carnot battery, considering low-grade industrial waste heat recovery [17]. A vapour injection technology was applied to the heat pump module, and a dual-pressure evaporation technology to the Organic Rankine Cycle (ORC) module. Compared with the conventional Carnot battery, the LCOS can be reduced by 26.7%. There are several studies on the modelling and numerical optimisation of Carnot batteries. However, only a few studies considered the geothermal part of the cycle in detail.

Systems utilising carbon dioxide (CO_2) or supercritical CO_2 (sCO_2) as the working fluid offer distinct thermodynamic advantages. CO_2 is a non-toxic, chemically stable, and significantly less expensive alternative to other heat transfer fluids [18]. Early conceptual work by McTigue et al. [19] established the superior power density of sCO_2 cycles, demonstrating that thermal integration with solar heat could drive round-trip efficiencies (RTE) toward 78%. As the technology moved toward commercial viability, Novotny V. et al. [20] provided a critical bridge between academic theory and industry, identifying CO_2 batteries as a "site-independent" and long-lived alternative to traditional pumped hydro. This was followed by a comprehensive system mapping by Shamsi et al. [21], who identified the near-ambient critical point of CO_2 (31.1 °C) as the key factor enabling compact, high-efficiency transcritical cycles. Recent research has shifted from steady-state feasibility to operational complexity; Tang et al. [22] explored the synergy between sCO_2 and industrial waste heat, while Girelli S. et al. [23] addressed economic barriers through "shared component" designs to reduce capital expenditures. Liang et al. [24] performed a thermo-economic assessment of a novel transcritical CO_2 Carnot battery integrating partial condensation, recompression, and waste heat recovery. Comparative results indicated that using CO_2/R32 zeotropic mixtures improves RTE by up to 12% over traditional sCO_2 recompression cycles. Economic modelling further estimated a payback period of 11.9 to 13.1 years, contingent upon regional factors, storage capacity, and waste heat availability. Finally, Chang et al. [25] evaluated a 6.8 MW high-temperature CO_2 heat pump Carnot battery designed for multi-energy cogeneration using thermal oil and water storage. Through dynamic modelling, the authors demonstrated that optimising compressor suction temperature and discharge pressure (to 400.15 K and 27.29 MPa, respectively) yielded a RTE of 50% while successfully providing simultaneous power, heat, and cooling. Although the study identified performance degradation in single-tank configurations due to thermal mixing during transient operation, it proved that transcritical CO_2 systems can maintain high performance under the fluctuating loads of modern decentralized grids. Transcritical CO_2 (tCO_2) cycles offer rapid response, high power density, and the ability to operate at relatively low temperatures compared to other conventional thermal cycles [26]. This configuration leverages the thermodynamic properties of CO_2 near its critical point, where it exhibits high energy density and excellent heat-transfer capacity [27]. The coupling of the heat storage and the heat pump or power cycle is a crucial design aspect. Guccione et al. [28] explored these couplings between the TES and a broad spectrum of power block configurations. A preliminary experimental investigation [29] addresses the design of a tCO_2 cycle for energy storage cycle, where the technical requirements and challenges for designing and operating a CO_2-based TES, as well as first experimental results, were presented. Collectively, these advancements position CO_2-based Carnot batteries as a cornerstone for future industrial decarbonization and multi-energy integration.

A recent evolution of the Carnot battery concept with transcritical CO_2 cycles has been the inclusion of geological CO_2 storage [30]. This concept combines thermal storage, energy conversion, and geological processes of CO_2 injection and production [31]. In this approach, CO_2 not only acts as the working fluid in the thermoelectric cycle but is also temporarily or permanently stored in underground geological formations [32]. The high-pressure and relatively low-temperature characteristics of transcritical cycles are well-suited to the integration of geological storage processes [33], allowing the desired conditions to be achieved without additional energy input [34]. This allows the system to have additional benefits, such as natural exploitation of the geothermal gradient or CO_2 fixation mechanisms [35]. This integration offers a seasonal storage solution with high energy density, leveraging carbon capture and storage (CCS) and the added value of utilising passive geothermal resources. The technology is currently under development, linked to the European Horizon Programme project " CO_2-based Electrothermal Energy and Geological Storage" (CEEGS) [36], which aims to provide scientific proof of the feasibility of the concept [37], addressing gaps in the interface between the surface transcritical cycle and underground CO_2 storage, and testing it at laboratory scale [38], raising the training readiness level to 4 (TRL-4). The system represents a convergence of thermal engineering, renewables, and geosciences, opening new avenues toward flexible, large-scale, and deeply coupled energy storage with the subsurface.

Despite the rapid progression in CO_2 Carnot battery research, several critical gaps remain. First, most current literature relies on "design-point" efficiencies, leaving a void in data regarding off-design performance and component behaviour during part-load operation. Second, existing studies often utilise simplified models for thermal storage; there is a distinct lack of research on the interactions between sCO_2 and complex geothermal reservoirs. Finally, the impact of high-pressure CO_2 on the large-scale installations has yet to be rigorously compared to competing technologies. This paper addresses a novel framework that utilizes pressurized CO_2 subsurface storage for long-duration capacity and thermal enhancement, providing a comprehensive system-level interpretation of long-term operational dynamics. While previous foundational research demonstrated the isolated optimisation of surface transcritical cycles [37] and preliminary steady-state wellhead couplings [34], the subsurface asset was treated as a static boundary condition. Conversely, this study addresses the critical gap of dynamic, fully coupled thermohydraulic evolution over extended operating horizons, where the surface plant and the underground reservoir actively interact. Using simulations of up to six months, this study identifies a transition period of 800 to 1,000 h required to reach a stable dynamic state, which is highly dependent on specific injection and production conditions. In addition, this work introduces practical operational criteria to guide the sizing of wells based on cavern size, while ensuring that the state of CO_2 stored underground is optimally coupled with the surface cycle for high-efficiency operation. Finally, the role of geothermal interaction is quantified and reframed as a key factor for thermal stabilisation and long-term safety, rather than as a primary energy source. This work extends previous studies by explicitly resolving the long-term thermo-hydraulic evolution of the integrated system over thousands of hours, providing new insights into the transition toward dynamic steady operation and the role of subsurface constraints on cycle feasibility. These contributions go beyond conceptual assessment to provide a robust framework for designing and deploying integrated energy storage systems.

2. Methods

This section describes the integrated numerical approach used to simulate the energy and geological storage system. It encompasses the configuration of the transcritical CO_2 cycles, the governing mathematical equations for (i) surface transcritical CO_2 cycles, (ii) geological injection and production processes, and (iii) the salt cavity, and the Python-based model validation.

2.1. CO_2-based electrothermal energy and geological storage system overview

The schematic of the energy and geological storage system analysed in this work is shown in Fig. 1. The electrothermal energy storage system is designed as a Carnot battery or reversible heat pump, which employs tCO_2 cycles and thermal storage as sensible heat on the high-temperature side (HT-TES) and as latent heat on the low-temperature side (LT-TES). The charging phase (conversion of electrical energy from renewable sources into thermal energy) involves compressing gaseous CO_2 to supercritical conditions, heat transfer in HT-hx, and supercritical cooling to dense-liquid conditions (below the critical temperature), followed by expansion and evaporation in LT-hx. The discharge phase (conversion of stored thermal energy into electricity) involves pumping liquid CO_2 above the critical pressure, heat transfer in HT-hx and heating under supercritical conditions, expansion in the power turbine to subcritical conditions, heat transfer in LT-hx and condensation of the CO_2.

On the surface, tCO_2 cycles can be connected to a PV plant as a renewable energy source, to the electrical grid, and to HT- and LT-TES. Underground CO_2 storage in one or more salt cavities, through one or more wells. The tCO_2 cycle of the charging phase can use a recuperative configuration by transferring heat between the expander inlet and the compressor inlet. The tCO_2 cycle for the discharge phase employs a simple configuration. Both cycles are connected to the HT- and LT-TES via heat exchangers. System balancing is achieved by additional heat input in LT-TES using a simple compression refrigeration cycle (Ref cycle). The CO_2 produced in the salt cavity is incorporated during the charging phase (4p in Fig. 1) after expansion and during the discharging phase (6p in Fig. 1) after pumping. CO_2 injection occurs after heat recovery during the charging phase (3* in Fig. 1) and before pumping during the discharging phase (5 in Fig. 1). The coupling between the transcritical CO_2 cycle and the wellhead requires a conditioning process [34], which involves expansion/compression, depending on the conditions.

The thermal and power components required in the proposed system are proven technologies, with a high degree of technological maturity, supported by their use in other industrial sectors [39]. Sensible heat exchangers can be designed in compact brazed-plate or microchannel configurations [40], widely used in supercritical Brayton cycles and ORC systems [41]. These printed circuit heat exchangers (PCHE) are very compact and cost-effective [42]. Here, channels are etched into steel plates stacked above one another and connected via diffusion bonding. The thermal–hydraulic characteristics and design optimisations of the PCHE have been studied in recent years, and more complex flow-channel structures have been applied to enhance heat-transfer performance [43]. The development of more generalised empirical correlations covering wide ranges of channel structures and flow conditions is an ongoing research activity, as flow behaviour for condensation or boiling heat transfer [44]. CO_2 evaporators and condensers operate under subcritical conditions, similar to those in commercial CO_2 refrigeration systems [41]. Conventional heat transfer equipment, using pipes for heat transfer, is a well-developed technology. The

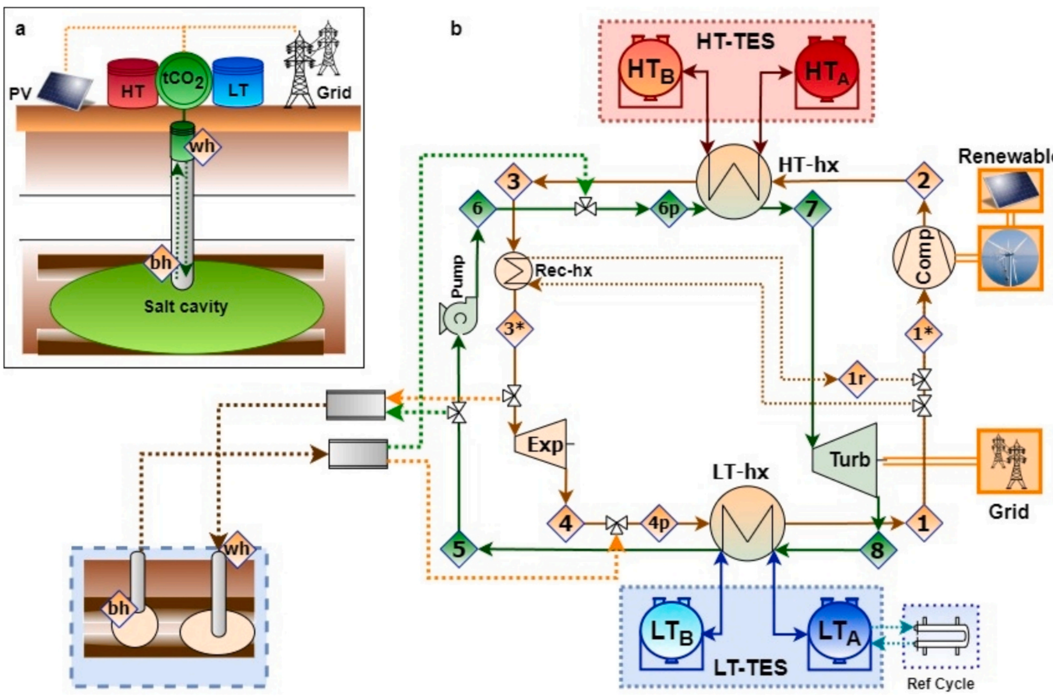

Fig. 1. Overview of the CO_2-based electrothermal energy and geological storage system. a) Simplified diagram of the system, differentiating between surface equipment (tCO_2 cycles and HT-, LT-TES) and underground CO_2 storage ('wh' refers to wellhead and 'bh' refers to bottomhole). b) Detailed diagram of the integration between the tCO_2 cycles of the Carnot battery and CO_2 storage in an underground saline cavity: charging phase (1-1r-1*-2–3-3*-4-4p) consisting of a recuperator (Rec-hx), expander (Exp), compressor (Comp) and heat exchangers (hx), connecting with the discharging phase (5–6-6p-7–8) which uses a pump and turbine (Turbine).

corresponding heat transfer and pressure drop correlations have been intensively developed in recent years for the relevant pressure and temperature ranges, and new correlations achieve a relative deviation of less than ± 20% [45]. Regarding power equipment, CO_2 compressors designed to operate at supercritical pressures (100–200 bar) are already used in applications such as CO_2 transport under supercritical conditions [46], industrial waste-heat valorisation [47] or power production [48]. Both centrifugal and reciprocating compressors can be used, with intercycle cooling and pulsation control [49]. Subcooled CO_2 pumps (dense liquid) are technically equivalent to those used in liquid CO_2 liquefaction and transport processes [50] and are characterised by their high volumetric efficiency and low specific consumption [51]. Liquid CO_2 expanders that recover useful work from pressure drops are being integrated into energy-recovery pilot plants in liquefied CO_2 distribution networks. Finally, turbines operating with supercritical CO_2 are part of the technological core of high-efficiency Brayton cycles, in both axial [52] and radial [53] designs. These turbines stand out for their compactness, high energy density, and reasonable dynamic control [54].

Thermal storage requires a good integration of the temperature profiles of CO_2 and the storage fluid. By using lightly pressurised water as the fluid in HT-TES, the system can benefit from its properties and the potential to reach temperatures above 100 °C. The tanks are typically made of carbon steel, thermally insulated, and designed as pressure vessels. It is a mature technology, used in district heating networks and industrial plants, with high efficiency (heat losses $<$ 1% per day) and low LCOS [55]. In the case of LT-TES, ice slurry storage exploits both the fluid's sensible heat and the ice's latent heat of fusion. With an operating temperature of −2 to 0 °C, the mixture of water and a eutectic solution (usually water-glycol) forms a suspension of ice microcrystals, which can be pumped and stored in insulated tanks [56]. The ice content can be 20–30% by mass, with an energy density of ~ 250 kWh/m3 (latent heat ~ 334 kJ/kg) [57]. Thermal losses can be around 1–3% per day with well-insulated tanks [58]. It has excellent thermal homogeneity and pipe transport capacity. This type of system is primarily used for refrigeration and air conditioning, though it is gaining interest in industrial applications due to its high thermal-discharge efficiency.

CO_2 storage in underground saline cavities has emerged as a promising solution for large-scale energy storage applications [59]. These cavities offer a sealed environment due to the impervious behaviour of salt rock and high geomechanical integrity [60], making them ideal candidates for containing pressurised fluids [61]. These cavities can operate at high pressures, usually close to lithostatic, and their high thermal conductivity allows for efficient recovery of stored thermal and mechanical energy [62]. However, temperature variations during gas injection and withdrawal cycles can influence the thermohydraulic behaviour of the surrounding salt formation. Previous studies have shown that temperature fluctuations associated with gas compression and expansion may generate thermal stresses, stress concentrations at the cavern walls, and long-term creep or thermo-mechanical fatigue effects in rock salt [63–65]. While these processes may affect cavern integrity during cyclic operation, they are not explicitly considered in the present study, as the objective is to analyse the thermodynamic performance and overall energy efficiency of the integrated surface and subsurface storage system. Salt cavities used for energy storage are often limited to depths of 2000–2500 m, where temperatures can be too high, the plasticity of the salt increases, and the cavity tends to close under its own weight. These advances suggest high scalability and cost-effectiveness potential for this type of energy storage, especially by reusing existing saline cavities and leveraging the availability of deep reservoirs in various regions worldwide.

The operation of the integrated electrothermal-geological storage system comprises different operating stages depending on the level of CO_2 stored in the salt formation: filling stage, cyclical stage, and shut-in stage. The filling stage is characterised by continuous CO_2 injection into the cavern, increasing the pressure in the salt cavity. It is aimed at establishing a cushion gas volume sufficient to maintain minimum pressure and ensure geomechanical stability of the cavity. This stage requires an external CO_2 source, such as a capture plant. The captured

CO_2 would arrive at the energy storage plant via pipeline or storage tanks, then pass through the transcritical TES cycle and be injected into the salt cavity. When the pressure in the cavern exceeds a minimum threshold (commonly based on lithostatic pressure) above the pressure induced by the cushion gas, the system can enter a cyclical operating stage. The CO_2 produced from the geological formation passes through the transcritical TES cycle and is finally injected back into the cavity. This process can be carried out in the same cycle, when two salt cavities are available, or in separate cycles using an auxiliary tank on the surface. It does not require an external CO_2 source. The system benefits from thermohydraulic storage and geothermal heat extraction, depending on the system characteristics (flow rates) and cavity size, as well as the operating mode (runtime). Finally, the system requires downtime during which it uses only closed-loop tCO2 cycles, excluding CO2 injection or production processes into the geological reservoir. These downtimes can range from hours to months. They can be motivated by various reasons, including maintenance issues or operational strategies to maintain thermal equilibrium between the injected CO2 and the higher-temperature salt rock, thereby increasing the temperature of the stored CO2 to enable greater heat extraction.

2.2. Mathematical modelling

A comprehensive model has been developed that encompasses three main components: (i) the charge and discharge phases of the surface transcritical CO_2 cycle, responsible for electric-to-electric energy conversion; (ii) the geological injection and production processes, which simulate the behaviour of CO_2 inside the well; and (iii) the salt cavity, which acts as geological scenario for overpressurised CO_2 storage. The approach adopted combines thermodynamic analysis, heat transfer, and simplified thermohydraulic simulations, enabling evaluation of the effects of parameters such as cavern depth, cavity volume, thermal cycle duration, and geological environment temperature. Each of these subsystems has been modelled in a coupled manner, accounting for realistic operating conditions and the detailed physical properties of CO_2. A numerical model has been developed in the Python language (version Python 3.12.7) and the open source CoolProp [66] library for the calculation of substance properties. These models have been used to evaluate the system's behaviour through numerical simulation.

2.2.1. Surface transcritical CO_2 cycles

The surface energy conversion system is based on two transcritical CO_2 cycles: one dedicated to the charging phase, in which electrical energy is converted into thermal energy and stored in the form of sensible (HT-side) and latent (LT-side) heat; and another corresponding to the discharge phase, where the stored thermal energy is reconverted into electricity through turbine expansion. A reference CO_2 mass flow rate of 30 kg/s is adopted; the water and ice mass flow rates required in the heat transfer systems, and the power of the main equipment are calculated from an energy balance, based on Eqs. (1)–(2).

$$\dot{Q}_{hx} = \dot{m}_{hot} \bullet \left(h_{in}^{hot} - h_{out}^{hot}\right) = -\dot{m}_{cold} \bullet \left(h_{in}^{cold} - h_{out}^{cold}\right) \tag{1}$$

$$\dot{W} = \dot{m} \bullet (h_{in} - h_{out}) = \dot{m} \bullet \Delta h \tag{2}$$

Where, $\dot{Q}_{hx}$ and $\dot{W}$ represent heat transfer rate in heat exchangers (kW_{th}) and mechanical power in compressors, pumps and turbines (kW), $\dot{m}$ is the mass flow rate (kg/s) and the subscripts 'in' and 'out' are the inlet and outlet conditions that define the specific enthalpy change (kJ/kg). The power equipment is modelled using an isentropic efficiency-based approach, using characteristic efficiencies reported in the literature for equivalent technologies under similar conditions [67]. The high-temperature side heat exchanges simulate the thermal coupling between supercritical CO_2 and pressurised liquid water. To accurately represent heat transfer, the nonlinear temperature profile of CO_2 during transcritical heating/cooling is considered, compared to the linear profile of water. The heat-exchange surface and thermal power are optimised by ensuring a minimum design temperature difference, which serves as a second-law constraint to avoid excessive irreversibilities. Heat transfer is performed in four stages to improve the integration of temperature profiles. Thermal exchanges on the low-temperature side, corresponding to the evaporation and condensation of CO_2, are coupled with the freezing and melting of water (0 °C), constituting the latent heat transfer stage. For these stages, a constant CO_2 evaporation temperature near –4 °C and a condensation temperature of 4 °C are assumed, with a minimum temperature difference of at least 4 °C to avoid thermal penalties. The CO_2 pressure on the LT side depends on the CO_2 phase-change temperature (evaporation during charging and condensation during discharging), according to the LT-TES phase-change temperature. The main assumptions in modelling the tCO_2 cycles are listed in Table 1.

To quantify electric-to-electric conversion efficiency, Eqs. (3)–(4) are defined, differentiating between the HT and LT sides. The indicators quantify the conversion of electrical energy from the perspective of the two TES temperature levels. The indicator is based on the ratio of the electrical energy generated during the discharging phase (heat engine mode operation – HE) to the electrical energy consumed during the charging phase (heat pump mode operation – HP). Considering that all the energy stored during the charging phase is used in the power production of the discharging phase [$\varnothing_{HP}^{HT,LT-TES} = \varnothing_{HE}^{HT,LT-TES}$], at each temperature level, the efficiency indicators depend only on the shape of the CO_2 transcritical charge–discharge cycles. Detailed mathematical development in references [34,37].

$$Eff_{LT}^{ele} = \frac{(\dot{W}_{HE}^{T} + \dot{W}_{HE}^{P}) \bullet \dot{Q}_{HP}^{LT-TES}}{(\dot{W}_{HP}^{C} + \dot{W}_{HP}^{Exp}) \bullet \dot{Q}_{HE}^{LT-TES}} \tag{3}$$

$$Eff_{HT}^{ele} = \frac{(\dot{W}_{HE}^{T} + \dot{W}_{HE}^{P}) \bullet \dot{Q}_{HP}^{HT-TES}}{(\dot{W}_{HP}^{C} + \dot{W}_{HP}^{Exp}) \bullet \dot{Q}_{HE}^{HT-TES}} \tag{4}$$

Where $\dot{Q}_{HP}^{XX-TES}$ and $\dot{Q}_{HE}^{XX-TES}$ refer to the thermal power (kW_{th}) in the HT-hx or LT-hx for each phase, charging and discharging. $\dot{W}_{HP,HE}^{X}$ is the power (kW) developed by the compression and expansion equipment, compressor (C), pump (P), expander (Exp) and gas turbine (T) in charging (HP) or discharging (HE) phases. This difference in efficiency across the overall conversion process establishes a range that depends on the thermal energy stored at each temperature level.

2.2.2. Injection and production processes

The developed well model allows simulation of CO_2 injection and production processes between the surface and an underground cavity,

Table 1
Main starting assumptions in the modelling of the surface tCO_2 cycles.

Parameter	Equipment	Value	Unit	Reference
Efficiency	CO_2 compressor	0.89	–	[26,37]
	CO_2 turbine	0.91	–	[26,37]
	CO_2 pump	0.86	–	[26,37]
	CO_2 expander	0.88	–	[26,37]
Minimum temperature difference	HT-hx	4	°C	[30,37]
	LT-hx	4	°C	[30,37]
Phase change temperature	LT-TES	0	°C	[26,37]
Number of stages	HT-TES	4	–	[37]
Charging cycle	CO_2 HT-Pressure	200	bar	[30,37]
Discharging cycle	CO_2 HT-Pressure	200	bar	[30,37]
CO_2 flow rate	Cycle	30	kg/s	[37]
Recuperative configuration	Rec-hx	100	%	[37,68]

accounting for thermal conduction into the geological environment. A one-dimensional, steady flow is assumed, with no accumulation of mass or energy along the well axis, as shown in Fig. 2.

The wellbore is represented as a vertical column, divided into 'n' segments of equal length (Δz). At each node 'i', the thermodynamic properties of CO_2 (pressure, temperature, density and enthalpy) are calculated using an equilibrium model for wellbore flow [69] and heat transfer [70] that takes into account depth, heat transfer with the surrounding geological formation, pressure losses and geothermal gradient, as shown in Eqs. (5)–(10).

$$\Delta h_i = g \bullet \Delta z + \frac{\Delta T_i}{R_{total,i} \bullet \dot{m}} \tag{5}$$

$$\Delta P_i = g \bullet \rho_i \bullet \Delta z + \Delta P_{loss,i} \tag{6}$$

$$R_{total} = R^{fluid}_{conv,i} + R^{tub}_{cond} + R^{ins}_{cond} + R^{cas}_{cond} + R^{cim}_{cond} + R^{gr}_{cond} + R^{fill}_{conv,i} \tag{7}$$

$$R_{cond} = \frac{\ln(r_o/r_i)}{k \bullet 2\pi\Delta z} \tag{8}$$

$$R_{conv} = \frac{1}{A \bullet hf_i} \tag{9}$$

$$\Delta P_{loss,i} = f_D \frac{L}{D} \bullet \frac{\rho_i \bullet v^2}{2} \tag{10}$$

Where Δh and ΔP represent the incremental increases in specific enthalpy (J/kg) and pressure (Pa), respectively, as a function of depth segment (Δz, m), and g is the acceleration due to gravity (m/s^2). The update of the thermodynamic state depends on the heat exchange area of each segment (A, m^2) and the mass flow of CO_2 ($\dot{m}$, kg/s), the wellbore radius (r_{well}, m) and a network of conductive (R_{cond}, K/W) and convective (R_{conv}, K/W) thermal resistances. Conductive resistance of the ground (R^{gr}_{cond}, K/W) depends on the thermal depth, a transient function of the geological formation thermal properties and the operation time. Pressure losses ($\Delta P_{loss,i}$, Pa) are estimated from the Darcy–Weisbach equation, where (f_D) is the dimensionless Darcy friction factor, L is the length of each segment (m), D is the tube diameter (m), ρ_i and v are the density (kg/m^3) and velocity (m/s) of the fluid, and hf_i is the convective heat transfer coefficient (W/m^{2}K).

2.2.3. Salt cavity

A thermohydraulic model has been developed to analyse the behaviour of CO_2 and the response of the surrounding wall of the saline cavity, considering the thermal effects induced by CO_2 injection and production. Although salt cavities are usually elongated in depth, for modelling purposes, the salt cavity is considered as a fixed-volume sphere that stores CO_2 under high-pressure conditions. See Fig. 3.

The purpose of this sub-model is to determine the thermodynamic state of the stored CO_2 over time, accounting for mass inflow and outflow, as well as heat exchange with the surrounding geological formation. The cavern is modelled as a rigid control volume (V = cte), in which the properties are uniform throughout the volume. Changes in kinetic and potential energy are considered negligible. The thermodynamic properties of CO_2 are evaluated using equations of state from the CoolProp library in Python. Although heat penetration in the

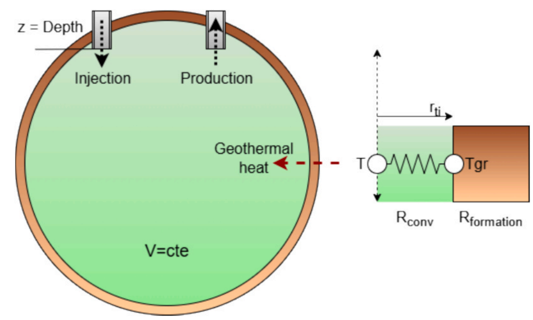

Fig. 3. Salt cavity modelling. The surrounding salt rock formation is characterized by a thermal conductivity of 5.6 W/m·K, a density of 2100 kg/m^3, and a specific heat capacity of 1120 J/kg·K. Heat transfer between the stored fluid and the surrounding rock salt is modelled as transient radial conduction from an infinite medium at geothermal temperature.

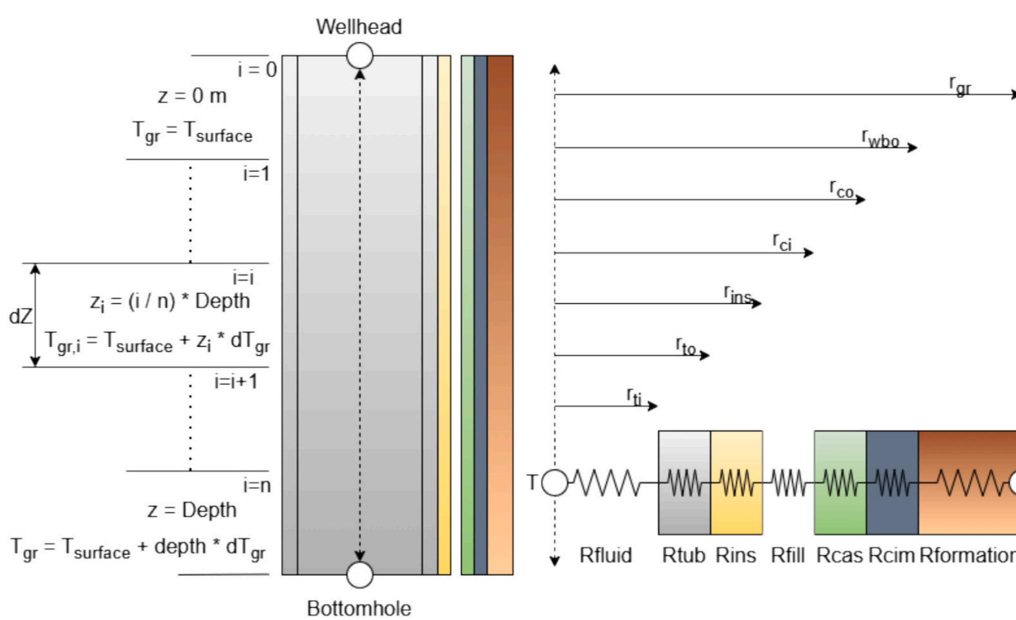

Fig. 2. Well modelling scheme: steel tubing characterised by a thermal conductivity of 45 W/m·K, an internal surface roughness of 50 μm, and a wall thickness equal to one-tenth of the tube's inner radius. Surrounding the tubing, thermal insulation is applied with a conductivity of 0.8 W/m·K and a thickness of 4 mm. The steel casing enclosing the well has a thickness of 10 mm. The cement layer between the casing and the geological formation is modelled with a thermal conductivity of 0.5 W/m·K and a thickness corresponding to one-sixth of the tube's outer diameter. The surrounding rock formation is characterised by a thermal conductivity of 1.73 W/m·K, a density of 2600 kg/m3, and a specific heat capacity of 902.7 J/kg·K.

surrounding salt rock is inherently transient, for the time scales considered, the thermal penetration depth is comparable to the cavern radius, and the rock mass can be modelled as an infinite medium at geothermal temperature. The energy balance depends on heat transfer with the surrounding geological formation, and injection and production are limited by time slots and pressure limits that vary with the depth of the cavern, as described in Eqs. (11)–(15).

$$\frac{dU}{dt} = \dot{m}_{in}h_{in} - \dot{m}_{out}h_{out} + \dot{Q}_{geo} \tag{11}$$

$$\frac{dm}{dt} = \dot{m}_{in} - \dot{m}_{out} \tag{12}$$

$$\dot{Q}_{geo} = \Delta T / R_{reservoir} \tag{13}$$

$$R_{reservoir} = \frac{1}{4\pi \bullet \mathrm{r} \bullet k} \tag{14}$$

$$\mathrm{u}_t = \mathrm{U}_t / M_{total,t} \tag{15}$$

Where dU represents the total internal energy increment (J) within the numerical time step dt (s), $\dot{m}_{in}$ and $\dot{m}_{out}$ the CO_2 mass flow rate (kg/s) during the injection (under bottomhole conditions – h_{in}, specific enthalpy in J/kg) and production (under the conditions of CO_2 stored in the salt cavity – h_{out}, specific enthalpy in J/kg) processes, and $\dot{Q}_{geo}$ represents the geothermal heat transfer rate from the rock formation walls (W_{th}). For a spherical cavern embedded in an infinite medium, the thermal resistance of the reservoir ($R_{reservoir}$, K/W) is inversely proportional to the cavern radius (r, m) and the rock thermal conductivity k (W/mK). Since the volume (m^3) is constant, the density (kg/m^3) evolves as $\rho = m/V$. The thermodynamic state of CO_2 is obtained by solving P=P (u,ρ), and T = T(u,ρ), using a real-gas equation of state, where 'u' is the specific internal energy (J/kg), U is the total internal energy (J) and M_{total} is the total mass (kg) of CO_2 stored in the cavern.

The governing equations are solved using an explicit Euler time integration scheme. The developed framework is flexible, allowing the implementation of any user-defined time step (Δt) depending on the computational criteria. To optimise computational efficiency while ensuring numerical accuracy across the different evaluation horizons of this study, the mathematical integration for long-term multi-cycle simulations (1-week to more than 6-month horizons) utilises a time step of Δt = 1 h. This 1-hour discretization is mathematically adequate for long-term multi-cycle horizons without sacrificing the accuracy required for short-term daily analysis. Since the plant scheduling could involve operational periods of 6–12 h or less, a 1-hour step provides sufficient resolution to capture the transient slopes, pressure peaks, and thermal responses of each operating phase without non-physical attenuation. This approach allows the model to accurately evaluate the cumulative impact of short-cycle operations over extended horizons while maintaining computational feasibility. These settings were verified through preliminary numerical sensitivity analyses (Δt = 15 min), which confirmed that decreasing the time step further yields overlapping and consistent thermodynamic trajectories, whereas utilising excessively large integration intervals triggers numerical oscillations and convergence issues due to the strong non-linearities of real-gas properties. The selected settings guarantee strict mass and energy conservation while ensuring computational feasibility over the extended operational horizon.

Table 2 shows the main assumptions made in the modelling of the salt cavity. The pressure limits will define the duration of the filling stage until the cavity reaches the reference pressure, and the characteristics of the injection and production cycles during the cyclic operation stage.

Table 2
Main starting assumptions in the modelling of the system.

Reference	Equipment	Value	Unit
Lithostatic pressure limits [71,72]	Lower limit (30%)	100	bar
	Reference (50%)	165	bar
	Upper limit (80%)	265	bar
Terrain	Geothermal gradient	30	°C/km
	Surface temperature	15	°C
Cavern	Size	100–10000	m^3
	Depth	1500	m

2.3. Validation of the model and limitations

The developed modelling framework combines validated approaches for each subsystem (surface cycles, wellbore flow, and subsurface storage) into an integrated system-level simulation. Given the lack of experimental data for the fully coupled concept, the validation strategy is based on component-wise benchmarking against well-established literature.

The surface thermal energy storage model is implemented in Python using the CoolProp library [66] and follows a methodology consistent with previous studies by the authors in the first integration of transcritical CO_2 cycles and salt cavities. [34] and in an in-depth study of all aspects of surface equipment, including recuperative configurations [37] and foundational works in transcritical CO_2 cycles of Morandin et al. [67] and Merchangoz et al. [26]. Using identical design parameters (isentropic efficiencies, pressure levels, and temperature pinch constraints), the model reproduces electric-to-electric efficiencies within a deviation below 1–2% compared to published results. This level of agreement provides confidence that the thermodynamic implementation correctly captures mass and energy balances and cycle performance. The thermal integration between CO_2 and the storage media (ice and hot water) is physically consistent, with minimum temperature differences (pinch points) maintained and no temperature crossings occurring. The obtained electric-to-electric efficiency range is highly consistent with similar tCO_2-based electrothermal systems.

The wellbore modelling framework has been previously applied and validated in the first study, considering salt cavities as a geological scenario in the CO_2-based thermal energy storage system using tCO_2 cycles [34]. Wellbore flow modelling is governed by the conservation equations formulated by Adams et al. [69], with 1% well discretisation uncertainty used, and similar values of 2.5 km, 0.27 m diameter well with a CO_2 mass flow rate of 170 kg/s, and velocity under 7.3 m/s, which is a kinetic energy change of 0.05% of the total energy change. Heat exchange with the surrounding geological formation follows the methodology proposed in Li et al. [70], accountings for the specific thermal properties of the completion materials—including steel casing, cement, and insulation—and the site-specific geological formation, following a methodology equivalent to that of the CO_2 injection/production reference studies [34]. The resulting pressure gradients, dominated by the hydrostatic column, are consistent with reported values in CO_2 injection studies and industrial-scale systems. Under comparable conditions, the model reproduces the expected pressure increase of approximately 12 MPa per 1000 m depth, while friction losses remain secondary.

The salt cavern is modelled using a lumped-parameter thermodynamic approach with transient radial heat transfer to the surrounding rock. This formulation is consistent with widely used models in CAES and CO_2 storage studies. The simulated pressure limits (30–80% of lithostatic pressure) and thermal behaviour are aligned with established geotechnical and thermodynamic guidelines for salt caverns. Despite this consistency, the model incorporates several simplifying assumptions that must be considered when interpreting the results. The cavern is represented as a rigid spherical volume with uniform thermodynamic properties, and the wellbore is modelled as a 1D system. These assumptions neglect localised spatial gradients and short-term transients, particularly near the wellbore interface. The salt cavity model is based on a thermohydraulic approach that accounts for mass and energy balances within a fixed-volume sphere. The transient heat exchange between the stored CO_2 and the surrounding rock salt is modelled as radial conduction into an infinite medium at geothermal temperature. This formulation considers the specific thermal properties of the formation: thermal conductivity, density and specific heat capacity. The reliability of the numerical integration, performed via an explicit Euler scheme, is supported by its consistency with analytical solutions for spherical heat transfer, where the increase in transfer area with radius compensates for the decreasing temperature gradient. The use of internal energy and density as primary state variables ensures numerical robustness under high-pressure real-gas conditions and guarantees energy conservation in the presence of mass injection and production. The modelling framework and the pressure-limit constraints have been previously successfully applied and reviewed in the context of CO_2-based energy storage systems, ensuring that the simulated thermodynamic states and thermal penetration depths remain within physically realistic and safe operational bounds [60]. Within the salt cavern, thermodynamic properties are assumed to be uniform. This lumped-parameter approach is physically justified by the high diffusivity and intense convective mixing induced by the high mass-flow injection of supercritical CO_2 over the simulated operational time scales. While localized thermal stratification or 3D flow effects near the wellhead may occur during rapid transitions, their impact on daily energy totals is negligible [74]. Furthermore, the rigid spherical cavern geometry provides a generalized representation of the subsurface volume. Although actual solution-mined salt caverns are typically elongated, the spherical approximation—which minimizes the surface-area-to-volume ratio—allows for a conservative estimate of geothermal heat exchange. This simplification is highly acceptable because the transient energy balance of the system is completely dominated by the mass inflow and outflow streams. Consequently, the long-term thermodynamic state of the stored CO_2 is governed by the global plant scheduling and charging/discharging cycles rather than the specific geometry of the cavity, using volume as a reference parameter [60]. This approach enables the simulation of extended operational horizons (over 4,000 h) with a manageable computational cost while providing a reliable, high-fidelity evaluation of the system's macro-level pressure and thermal boundaries [71]. Furthermore, the operational pressure limits for the salt cavity are strictly defined between 30% and 80% of the lithostatic pressure, following the maximum and minimum pressure values used as pressure limits in the compressed air energy storage (CAES) industry [71,72], ensuring CO_2 remains in a supercritical state while preventing sealing loss or cavity closure, following established geotechnical guidelines for salt caverns. The maximum depth of the salt cavity would be the same as typically recommended for CAES or natural gas storage, which is 2500 m, to avoid salt plasticity at high temperatures [72]. The consistency of these models with existing literature on CO_2 plume geothermal systems and CAES provides the necessary reliability for the analysis of the integrated system. The results show that the global energy balance is dominated by mass inflow and outflow (8–10 MW), while geothermal heat transfer remains below $\sim$ 20 kW under cyclic operation (<0.25% of the energy balance). Therefore, the impact of spatial heterogeneity on system-level performance is expected to be limited.

The comprehensive model exhibits appropriate robustness for system-level evaluation, although the current modelling framework incorporates several simplifying assumptions. Regarding transient behaviour, the combined effect of the 1D wellbore and lumped-parameter assumptions may slightly smooth out localized, short-lived pressure and temperature peaks during rapid operational transitions. Nevertheless, due to the high compressibility and fast thermal diffusivity of dense sCO_2, these localised gradients attenuate rapidly without altering daily energy totals. Furthermore, the spherical cavern approximation establishes a thermally conservative baseline by minimizing the heat transfer area, ensuring that the system's operational safety margins regarding overpressurisation or thermal fatigue are not overstated. Consequently, the integrated framework remains highly accurate for establishing macro-level plant scheduling and global efficiency boundaries. Furthermore, the simulation parameters and time steps were selected and coupled to ensure the numerical model operates within its mathematical stability limits. This mathematical stability directly reflects the physical design requirements of the system, where the cavern volume, mass flow rates, and plant scheduling parameters are strictly interrelated. By properly calibrating these operational variables against the thermal and volumetric inertia of the cavern, the numerical framework effectively handles the strong non-linearities of supercritical CO_2 real-gas properties. With this configuration, the numerical framework strictly adheres to the fundamental laws of mass and energy conservation throughout the long-term (over 1000 h) simulation horizon, successfully achieving an optimal balance between numerical accuracy and computational speed. The present framework should be interpreted as a first-order, system-level model, suitable for analysing long-term operational trends, pressure constraints, and energy balances, but not for resolving detailed local thermofluid or geomechanical phenomena.

3. Results

The results section presents the performance of the proposed system, coupling the transcritical surface thermal energy storage cycle, injection and production processes, and underground saline formation. The following subsections analyse its operational phases, from surface energy conversion to underground storage dynamics, detailing cycle efficiencies, the transient behaviour of CO_2 within the saline cavern, the effect of depth, and the long-term impact of geothermal heat exchange relative to cavern size.

3.1. *Transcritical CO_2 cycles as an energy storage and power generation system*

Fig. 4 presents the results related to the tCO_2 cycles operating in isolation mode, as a conventional Carnot battery. Fig. 4a shows the temperature–entropy (T–s) diagram of the transcritical CO_2 cycles used in the system, operating in charge and discharge modes. In the charge phase, CO_2 evaporates at -4 °C at a pressure of 31.3 bar, while in the discharge phase it condenses at 4 °C at a pressure of 38.7 bar. Heat exchange in LT-hx maintains a minimum temperature difference of 4 °C. Thermal storage in the LT-side releases and absorbs latent heat at a constant temperature of 0 °C. Both phases operate at a pressure of 200 bar on the HT side. In the charge cycle, a recuperative configuration with an internal heat exchanger is used to increase the fluid temperature before compression, thereby improving process efficiency. The compressor outlet temperature reaches 192.6 °C, the highest in the system. The turbine inlet temperature is 167.1 °C. The temperature values and cycle shape are almost identical to those presented in the recuperative configuration in [37], considering the pressure values mentioned above. The heating at the compressor inlet is conditioning the turbine outlet, whose expansion line shifts to the right in the diagram, away from the saturation bell. The coupling point with geological injection would be in the dense liquid zone, after supercritical cooling in the charging phase (200 bar, 8.5 °C) and after condensation in the discharging phase (38.7 bar, 4 °C, saturated liquid). The CO_2 conditions at the coupling point of the production process must be similar to those at the inlet of the evaporator in the charging phase (31.3 bar, -4 °C, saturated liquid) and those at the inlet of the supercritical heating in the discharging phase (200 bar, 28 °C).

Fig. 4b-c represents the power balance of both cycles, differentiating between thermal (red bars – cooling and blue bars – heating) and electrical (green bars – compression and yellow bars – expansion) powers. In the charging phase (Fig. 4b), the compressor accounts for the largest energy consumption ($\sim$3.5 MWe), achieving heat transfer of $\sim$ 10 MW_{th} in HT-hx and $\sim$ 7 MW_{th} in LT-hx. In the discharging phase

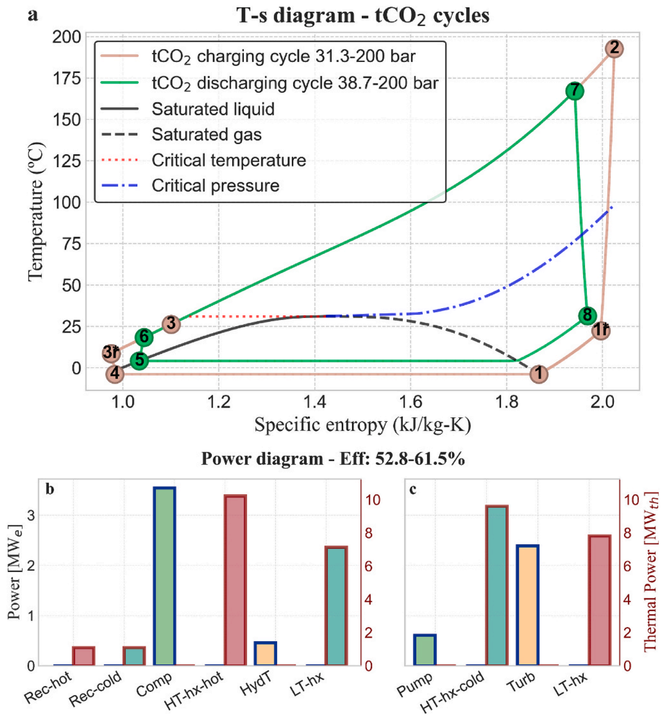

Fig. 4. Transcritical CO_2 cycles as an energy storage and power generation system: a) T-s diagram of the charging phase (brown) and discharging phase (green), b) Power diagram in the charging phase, and c) Power diagram in the discharging phase. Description of the charging cycle: (1-1r) Heating in the recuperator (Rec-hot), (1r-2) compressor (Comp), (2–3) cooling of sCO_2 (HT-hx-hot), (3-3r) cooling in the recuperator (Rec-cold), (3r-4) expander (Exp), (4–1) evaporation of CO_2 (LT-hx). Description of the discharging phase: (5–6) pump (Pump), (6–7) sCO_2 heating (HT-hx-cold), (7–8) turbine (Turb), (8–1) CO_2 condensation (LT-hx).

(Fig. 4c), the turbine generates approximately 2.4 MWe, with heat transfer of ~ 9.6 MW_{th} from HT-hx and ~ 7.8 MWth from LT-hx. The recuperative cycle achieves an electric-to-electric conversion efficiency of 52.8% to 61.5%, depending on how the excess thermal energy is managed on the HT side relative to the LT side. This value is above the simple cycle configurations' efficiencies of 42.4–53.9% [30], and 48.3–56.4% [37], and in the same range in which it is placed, the recuperator configuration case in [37], in which the electric-to-electric efficiency would be in the range of 52.6–61.4%, and the round-trip efficiency would be 57.9% using an ammonia refrigeration cycle for balancing. The efficiency range relates the time during which the discharging phase can operate to the operating time of the charging phase. The mass flow rate in both cycles is the same (30 kg/s). The available operating time of the discharging phase (available discharging hours) can be adjusted based on the mass flow rate ratio between phases, which is directly related to the equipment's power.

The results show the consistency of the surface cycle model when compared with reference cases, published results and validated simulations of the foundational cases of Morandin et al. [67] and Merchangoz et al. [26], as well as previous studies on integrated storage by Carro et al. [30,31]. The model's reliability is confirmed by the high degree of consistency in design parameters and results: using identical isentropic efficiencies (0.85 for compression and 0.90 for expansion), a high-pressure limit of 200 bar, and a 4 °C pinch point, the obtained electric-to-electric efficiency range (52.8%–61.5%) aligns with the 60.0% reported by Morandin et al. [67] and the 52.6%–61.4% range validated for recuperative cycles in [37]. The thermal integration between CO_2 and the storage media (ice and hot water) is physically consistent, ensuring no temperature crossings occur. This quantitative agreement across all thermodynamic nodes and performance indicators demonstrates the robustness of the surface cycle implementation for system-level analysis.

While the electric-to-electric efficiency (52.8–61.5%) is primarily determined by the surface transcritical CO_2 cycles, the subsurface system plays a critical indirect role by constraining the thermodynamic state of CO_2 at the wellhead. In particular, the pressure and temperature conditions within the salt cavern directly affect the feasibility of achieving the required inlet conditions for the LT and HT heat exchangers. When cavern pressure approaches the lower limit, the produced CO_2 tends to shift toward gaseous conditions, leading to suboptimal integration with the surface cycle. Conversely, operation near the upper pressure limit maintains CO_2 in a dense supercritical state, which enables more favourable thermodynamic matching. Therefore, although the underground processes contribute negligibly to the total energy balance in terms of direct power exchange, they play a fundamental role in defining the operational envelope of the system and, consequently, the achievable cycle efficiency.

3.2. *Salt cavity as the geological reservoir*

This section presents the results of the temporal simulation of the integrated system, analysing the behaviour of CO_2 stored inside a saline cavity. The cavern, with a volume of 10,000 m^3, is located at an average depth of 1600 m. A tube diameter of 30 cm and a mass flow rate of 30 kg/s are considered in wells, with a vertical profile that accounts for the fluid's thermodynamics as it descends or ascends. In the analysis of the production process, the CO_2 stored in the cavern is initially considered to be in thermal equilibrium and at the reference pressure (50% of the lithostatic pressure) corresponding to the depth. The injection conditions at the wellhead are those required to achieve a pressure slightly higher than that of the CO_2 stored in the geological formation. Fig. 5 shows the numerical simulation of CO_2 behaviour during the injection process through the well connected to the salt cavity.

Fig. 5a analyses the temperature and thermal power of the process. Heat transfer increases with depth, depending on the temperature difference between the fluid and the ground. Both the fluid temperature (blue) and the ground temperature (orange) increase with depth. Although the thermal power is negative until almost halfway down the well, the fluid temperature increases throughout the process due to the increase in pressure with depth, which is the dominant process in the energy balance. Heat transfer also depends on thermal insulation, which is not governed by convective resistance (Fig. 5b). Pressure increases with depth due to the weight of the fluid column, rising from about 60 bar at the surface to almost 180 bar at the bottom. See Fig. 5c. Gains per gravitational column (blue) are the dominant factor, while friction losses (red) are negligible (close to zero). Fig. 5d shows the evolution of density (blue) and velocity (green). As pressure increases with depth, the fluid compresses, increasing its density from ~ 720 kg/m^3 to ~ 790 kg/m^3. Due to the conservation of mass, as the fluid becomes denser at the bottom, its velocity decreases (~0.54 m/s). Pressure in the injection process is dominated by gravity (hydrostatic column), where the fluid increases in temperature and density as it descends, reducing its velocity. These results are consistent with those obtained in similar studies [34]. At the bottom of the well, CO_2 is under supercritical conditions, with a pressure of approximately 185 bar and a temperature of 45 °C. The bottomhole conditions obtained (185 bar and 45 °C) are remarkably consistent with the theoretical peak power envelopes for sCO_2 turbines installed at 1500 m depth reported by Minkley et al. [60], where similar pressure levels are required to maintain the supercritical state and maximize mechanical energy storage. Pressure evolution in the injection well is similarly dominated by the gravitational column. Specifically, for a vertical depth of 1500–1600 m, both models report a pressure increase from surface conditions (~60 bar) to approximately 180 bar at the bottomhole. The negligible impact of friction losses (< 2 MPa) and the evolution of CO_2 density (from ~ 720 to ~ 790 kg/m^3) are in full agreement with the thermodynamic trajectories validated for salt dome

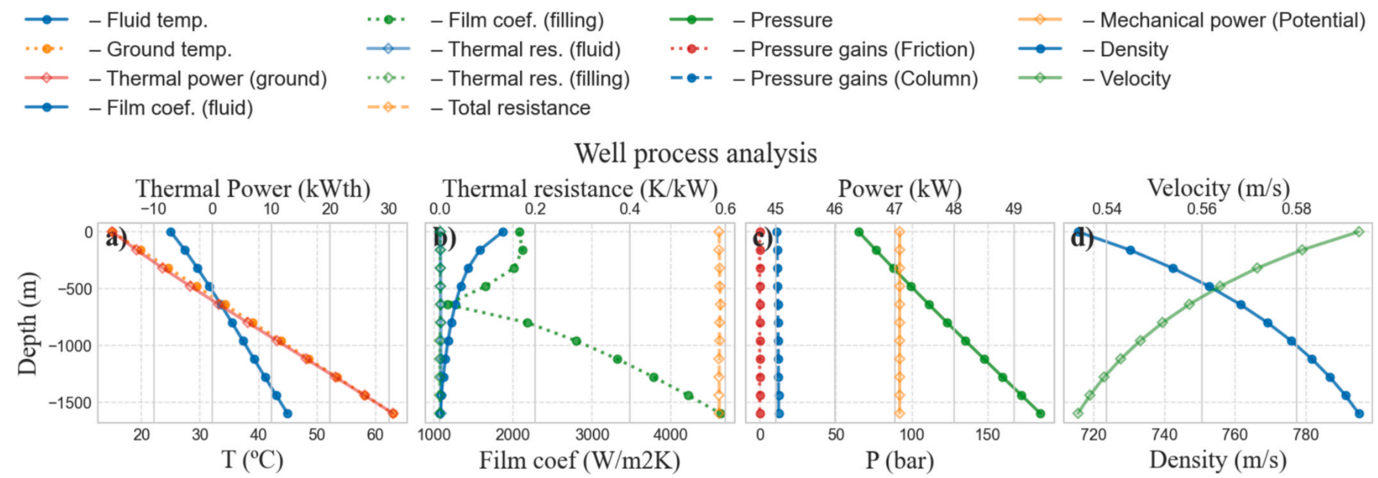

Fig. 5. CO_2 injection into a 1600 m depth salt cavity: a) Heat transfer (temperature and thermal power), b) Transfer properties (thermal resistances and form coefficients), c) Mechanical power (pressure evolution and power as a function of depth), and d) Fluid behaviour (velocity and density).

storage in. The total mechanical power of the injection process would be around 518 kW, in the order of magnitude of the transcritical surface cycle pump or expander (dense zone), compared to the 69.4 kW of thermal power exchanged with the ground, far from the 7–10 MW_{th} of HT-hx and LT-hx.

Considering a plant schedule of 6-hour periods, in which the injection and production processes operate every day with the same mass flow rate (30 kg/s), from 6 am to 12 pm and from 12 pm to 6 pm, respectively, the contribution of the injection and production processes is presented in the energy balance in Fig. 6, over a period of one week (approximately 170 h). The temporal resolution is designed to address the inherent intermittency of renewable energy sources. A 6-hour operational cycle is adopted to represent the standard charging (surplus) and discharging (demand) windows of solar and wind energy.

Fig. 6a presents the time evolution of the pressure (green) and density (brown) of the stored CO_2. A cyclic behaviour is observed, depending on the operating periods of the injection and production processes, with pressure peaks reaching up to 260 bar. The baseline pressure level gradually decreases, approaching the cavern's lower pressure limit. The conditions at the wellhead depend directly on the conditions in the subterranean geological formation, determining the efficiency of the entire system. The density follows the pressure profile, oscillating between approximately 655 and 720 kg/m3, depending on the mass of CO_2 stored within the salt cavern. Fig. 6b shows the time evolution of the stored CO_2 temperature and the thermal power of the energy balance. The temperature (orange) shows a cooling trend due to the lower temperature of the injected CO_2. The maximum temperature drops from around 75 °C to about 55 °C in the last, while the minimum reaches 40 °C. The temperature is governed by injection and production processes, with geothermal gains playing a secondary role. The mass (Fig. 6c) oscillates between approximately 6550 and 7200 tonnes of CO_2 (increments of approximately 10%). The equivalent power peaks of the rate of change of internal energy are in the 8–10 MW range, well above the 20 kW thermal power peaks from geothermal gains. The simulated thermal response—characterized by a cooling trend from 75 °C to 40 °C due to cyclic injection—is consistent with the long-term coupled thermohydraulic behaviour reported by [60] for supercritical CO_2 storage. The identification of geothermal gains (~20 kW) as a secondary factor compared to the dominant mechanical power (8–10 MW) aligns with the findings in, where the subsurface acts primarily as a thermal buffer.

The difference between the energy gains from the injection and production processes and the progressive loss of temperature and pressure associated with them indicates that the amount of CO_2 stored in the cavern could increase over time until a certain level is reached that will determine the plant's schedule, keeping pressure levels within the cavern limits. Fig. 7 shows the temporal evolution over a period of six months (approximately 4350 h) in two cases: injection mass flow equal to production of 30 kg/s of CO_2, and an injection mass flow of 30 kg/s, greater than production of 25 kg/s. Comparing the short-term simulation (170 h) with the new long-term simulation (4350 h), we observe the system transitioning from an initial transient phase to a state of dynamic equilibrium, or steady state.

In the first case (Fig. 7-left), a progressive pressure drop is observed until the lower limit is reached, after which the operating periods of the production process are restricted. As the mass stored in the cavern increases, density also rises, shifting from peaks of 720 kg/m3 at the start to nearly 780 kg/m3 by the end. In the long term, thermal stabilisation is observed. While the temperature showed a "free-fall" in the short term, suggesting continuous cooling, the long-term data reveal that after the first 800 h, the temperature ceases to drop and stabilises within a constant oscillatory range (between 35 °C and 50 °C). This indicates that the system acquires a new state of dynamic equilibrium, governed by the injection and production processes rather than by the terrain's geothermal gradient. In the second case (Fig. 7-right), the equilibrium state is reached at approximately the same time (~1000 h), with different operating parameter values but the same trend. The pressure change occurs incrementally toward the upper pressure limit of the cavern. This is associated with an increase in the cavern's storage capacity, which stabilises at around 8300 tonnes of CO_2, up from 7750 tonnes in the previous case. In this case, the operating periods of the injection process are restricted. Thermally, the temperature stabilises in the 40 °C to 55 °C range, slightly higher than the 35–50 °C range observed previously.

The new dynamic steady state, occurring around 800–1,000 h, defines the representative operational regime of the energy storage system. The salt cavern's energy balance is dominated by the injection and production streams (8–10 MW), which depend on the wellhead conditions during injection, the mass flow ratio, and the operating period. Considering daily injection–production cycles, a mass flow rate that allows for 10% oscillations in the total mass of stored CO_2 (at reference conditions) is an appropriate criterion for wellbore sizing based on the salt cavern volume. This ensures that the pressure remains within safety limits. The ratio between the injection and production mass flow rates drives the system towards its upper or lower lithostatic limits, which ultimately necessitate operational restrictions on the duration of the injection (upper limit) and production (lower limit) processes. The wellhead injection pressure must be set such that, following the injection process (governed by the pressure increase relative to depth), the bottomhole pressure matches the cavern's requirements according to the oscillations. Consequently, once the wellhead injection pressure is

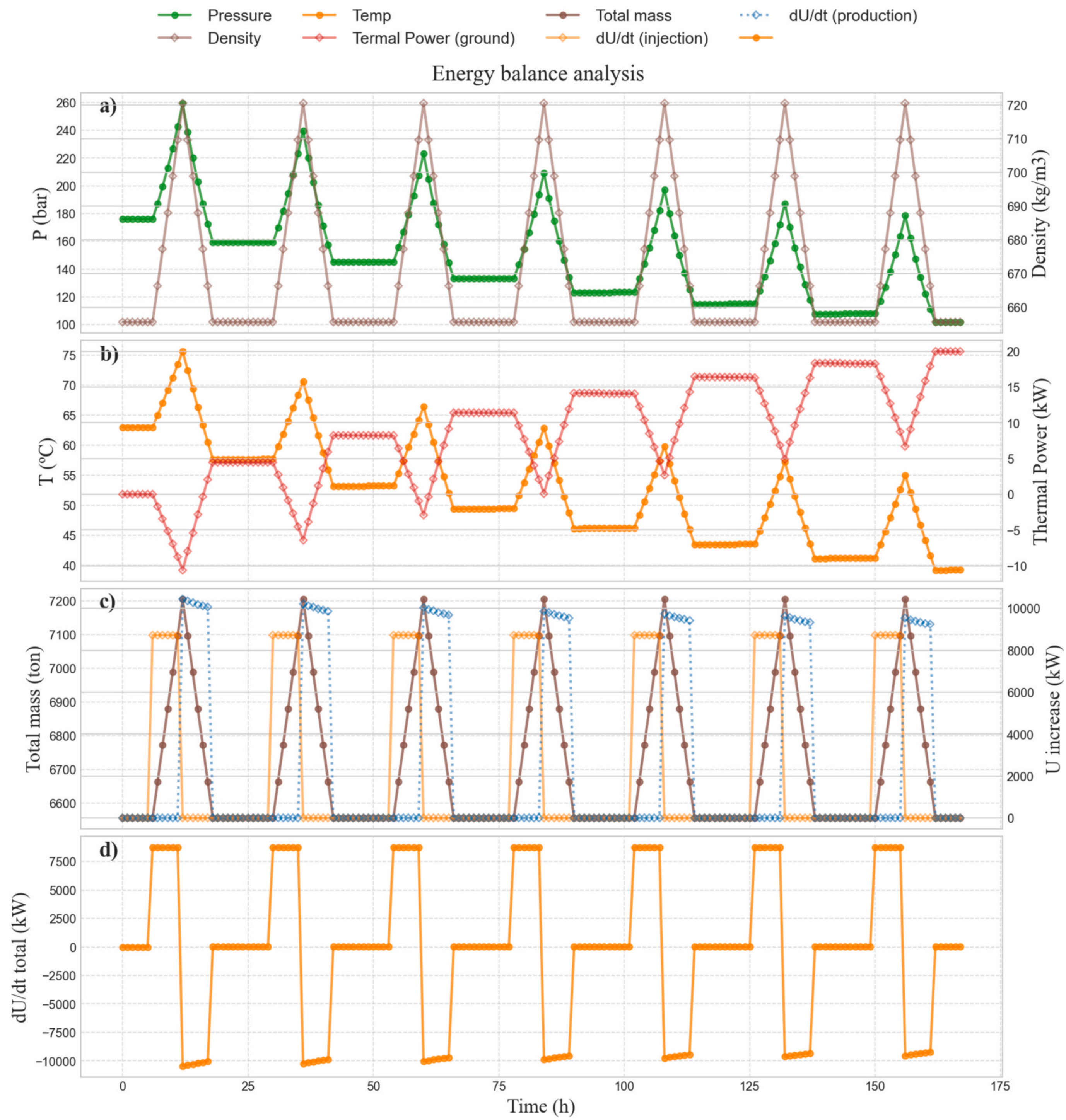

Fig. 6. Temporal analysis of the energy balance in the salt cavity over a period of one week, alternately using injection and production processes in 6-hour intervals, respecting the pressure limits of the cavern: a) Mechanical energy storage (pressure and density), b) Geothermal gains (temperature and thermal power), c) Impact of injection and production (CO_2 mass and energy increases), and d) Increase in total internal energy.

fixed, the formation temperature at thermal equilibrium can be controlled by the wellhead injection temperature, taking into account the formation depth. The output of the injection process is a significant parameter for the efficiency of the transcritical CO_2 cycle. Performance indicators, such as electric-to-electric conversion efficiency, must be evaluated during this stabilised dynamic phase to reflect the plant's long-term viability accurately. Table 3 presents the energy balance taking into account the two simulated scenarios, in which the new dynamic equilibrium lies at either the lower or upper limit, and the mass flow rate of CO_2 produced/injected is 50% of the mass flow rate of CO_2 passing through the compressor during the charging phase and the turbine during the discharging phase.

The state of CO_2 stored within the salt formation directly impacts the efficiency of the transcritical CO_2 energy storage cycle. In cases where the pressure fluctuates around the lower limit, the temperature and pressure conditions of the CO_2 may enter the gas-supercritical transition zone. At the production wellhead, the CO_2 is at around 30 bar and temperatures below 0 °C, within the two-phase region. Coupling in the

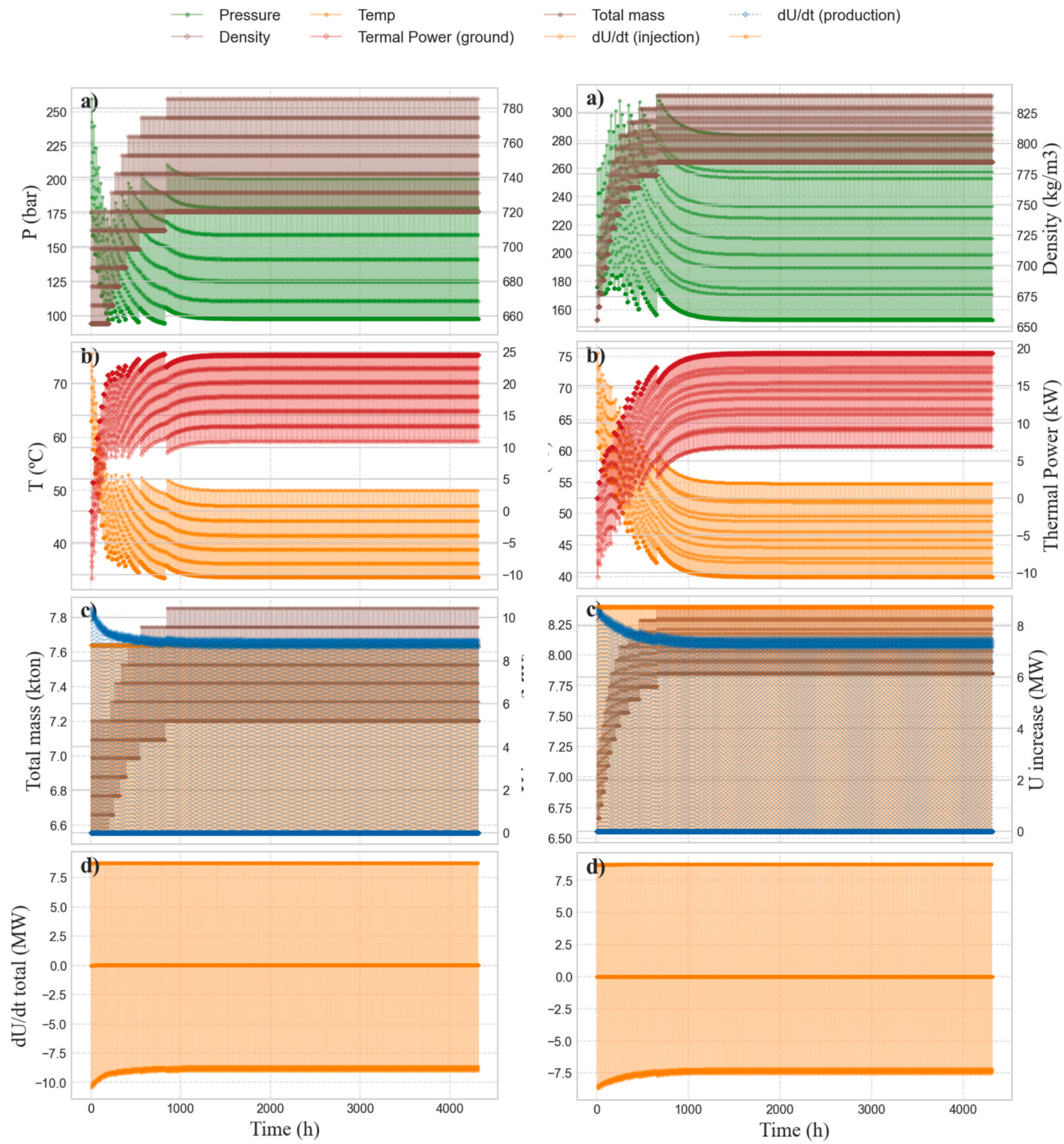

Fig. 7. Temporal analysis of the energy balance in the salt cavity over a period of six months, alternately using injection and production processes in 6-hour intervals, respecting the pressure limits of the cavern in two cases: 30 kg/s CO_2 flow rate in injection and production [left], and 30 kg/s CO_2 flow rate in injection and 25 kg/s CO_2 flow rate in production [right]; a) Mechanical energy storage (pressure and density), b) Geothermal gains (temperature and thermal power), c) Impact of injection and production (CO_2 mass and energy increases), and d) Increase in total internal energy.

charging phase would set the vapour quality at 0.39, significantly reducing heat transfer in the LT-hx and thermal energy transfer to the LT-TES. In the case of the discharging phase, the coupling involves significant compression from the two-phase region, which raises questions regarding feasibility, or prior condensation that increases the thermal requirements from the LT-hx. Both options reduce the cycle efficiency on the LT side, which would be in the range of 36.2–60.5%. Conversely, when the pressure approaches the upper limit, the CO_2 stored in the salt cavern is under supercritical conditions, within the dense region of the diagram. Following production (153.4 bar, 38.8 °C), expansion brings the fluid to suitable conditions (vapour quality of 0.18) for entry into the LT-hx during the charging phase, and effective pumping of dense supercritical fluid (150 bar, 22 °C) during the discharging phase. Injection would provide the system with the capacity to

Table 3
Power balance in the equipment in two states of dynamic equilibrium: pressure at the lower limit and at the upper limit.

Process	Pressure in the lower limit			Pressure in the upper limit		
	Inlet	Outlet	Power	Inlet	Outlet	Power
Production	105 bar	29 bar	−259 kW	281.5 bar	153.4 bar	−259 kW
	35 °C	−6.8 °C (0.4)	218 kW_{th}	55 °C	38.8 °C	−81.5 kW_{th}
Expander/Pump LT	29 bar	31.3 bar	−21.8 kW	153.4 bar	31.3 bar	205.2 kW
	−6.8 °C (0.4)	−4 °C (0.39)		25 °C	−4 °C (0.18)	
LT-hx Evaporator	31.3 bar	31.3 bar	5786.6 kW_{th}	31.3 bar	31.3 bar	6550.7 kW_{th}
	−4 (0.2)	−4 (1)		−4 (0.1)	−4 (1)	
Compressor	31.3 bar	200 bar	3545 kW	31.3 bar	200 bar	3545 kW
	22.2 °C	192.6 °C		22.2 °C	192.6 °C	
HT-hx Cooling	200 bar	200 bar	−10219 kW_{th}	200 bar	200 bar	−10219 kW_{th}
	192.6 °C	26.2 °C		192.6 °C	26.2 °C	
Expander HT	200 bar	45.3 bar	210.8 kW	200 bar	135 bar	89.7 kW
	8.5 °C	10 °C	439.3 kW_{th}	8.5 °C	10 °C	170 kW_{th}
Injection	45.3 bar	183 bar	259 kW	135 bar	283 bar	259 kW
	10 °C	28.5 °C	190.3 kW_{th}	10 °C	25.8 °C	203.5 kW_{th}
Production	105 bar	29 bar	−259 kW	281.5 bar	153.4 bar	−259 kW
	35 °C	−6.8 °C (0.4)	218 kW_{th}	55 °C	38.8 °C	−81.5 kW_{th}
Pump HT	29 bar	200 bar	−545.3 kW	153.4 bar	200 bar	−90 kW
	−6.8 °C (0.4)	58.3 °C		22 °C	26.3 °C	
HT-hx Heating	200 bar	200 bar	8249.8 kW_{th}	200 bar	200 bar	9347.5 kW_{th}
	39.1 °C	167.1 °C		22.3 °C	167.1 °C	
Turbine	200 bar	38.7 bar	2389.7 kW	200 bar	38.7 bar	2389.7 kW
	167.1 °C	31.2 °C		167.1 °C	31.2 °C	
LT-hx Condenser	38.7 bar	38.7 bar	−7818 kW_{th}	38.7 bar	38.7 bar	−7818 kW_{th}
	31.2 °C	4 °C (0)		31.2 °C	4 °C (0)	
Pump LT	38.7 bar	45.3 bar	−12.8 kW	38.7 bar	135.9 bar	−184.4 kW
	4 °C	10 °C	222.8 kW_{th}	4 °C	13 °C	
Injection	45.3 bar	183.1 bar	259 kW	135.9 bar	283.6 bar	259 kW
	10 °C	28 °C	190.3 kW_{th}	13 °C	28.3 °C	177.5 kW_{th}

store approximately 450 kW of mechanical power, in addition to the 6–10 MW_{th} in each heat exchanger. The selection of appropriate storage conditions within the salt cavern ensures that the transcritical CO_2 cycle configuration is optimised to operate with high electricity-to-electricity conversion efficiencies, reaching the range of 50.3–65.6%.

The storage pressure and temperature must be suitable to allow adjustment of conditions from the wellhead to states approaching the dense liquid phase at the inlet of the LT-hx during charging, or at the inlet of the HT-hx during discharging. High pressure values, with greater importance, and temperature, enable a conditioning process involving ambient cooling to shift the CO_2 towards the dense region of the property diagrams before its pressure is adjusted. Consequently, for an optimal surface–subsurface coupling, actively controlling the thermodynamic state of the stored CO_2 is crucial.

3.3. Depth in CO_2 injection and production processes

Fig. 8 presents the results from the numerical simulation of CO_2 behaviour during the production and injection processes through a well connected to a salt cavity. The analysis focuses on a depth range between 1,000 m and 2,500 m, encompassing both the evolution of the fluid's thermodynamic properties and the associated energy gains. The same wellhead inlet conditions of 120 bar and 20 °C are used for the injection process. The simulation shows the behaviour of the fluid within the well, enabling analysis of how key variables such as pressure, temperature, velocity, and density evolve. Energy gains, such as specific enthalpy, heat transfer, potential energy, and friction losses, are quantified.

Fig. 8a shows the evolution of the thermodynamic properties of CO_2 as it ascends through the production process. A progressive decrease in pressure is observed, consistent with the fluid expanding as it rises in the well. The temperature decreases along the wellbore due to the negative geothermal gradient and cooling from expansion. The density decreases, consistent with fluid expansion, as the pressure decreases. The velocity increases due to the expansion of CO_2 and the reduction in density. At depths below 1500 m, an abrupt change in the trend of the density and velocity curves is observed because the pressure and temperature are below the critical point, and the CO_2 enters the saturation bell (biphasic). During the injection process (Fig. 8c), the pressure increases almost linearly with depth, due to the weight of the fluid column and the progressive compression. The temperature also increases with depth, driven by the geothermal gradient and compression. The combination of both effects causes the density (and velocity) to evolve differently depending on the section of the well analysed. Depending on the depth, the injection wellhead conditions must be tailored to achieve the appropriate state within the salt formation during the dynamic steady state. This ensures the desired production wellhead conditions required for a high-efficiency transcritical CO_2 energy conversion cycle.

3.4. Cavity size and geothermal heat effects

Fig. 9 shows the time evolution of pressure (a) and temperature (b) of CO_2 confined in an underground cavern, considering different storage capacities, represented by the volume of the cavern (from 100 to 10,000 m^3). All scenarios start from common initial conditions (depth of 1500 m, reference pressure of 165 bar and temperature of 40 °C, lower than that of the geological formation) and are subjected to a constant geothermal environment. The total simulation duration is extended to 4,350 h (6 months) to ensure that the performance metrics reflect the system's behaviour, accounting for the long-term thermal interaction between the stored CO_2 and the geological formation.

Both graphs show that smaller caverns experience faster, more significant increases in pressure and temperature. From a thermodynamic perspective, these results reflect the damping effect of the thermal mass associated with larger fluid volumes. This implies that systems with smaller storage capacity respond more quickly to the thermal gradient of the geological environment. Although geothermal heat transfer are negligible compared to those from the operational fluid streams, during prolonged shutdown periods, when mass flows drop to zero, these accumulated thermal gains become significant and must be taken into account, as the slow rise in pressure driven by the thermal gains could affect the cavern’s safety limits. The pressure increase resulting from this phenomenon could lead to the upper pressure limit of the cavern being

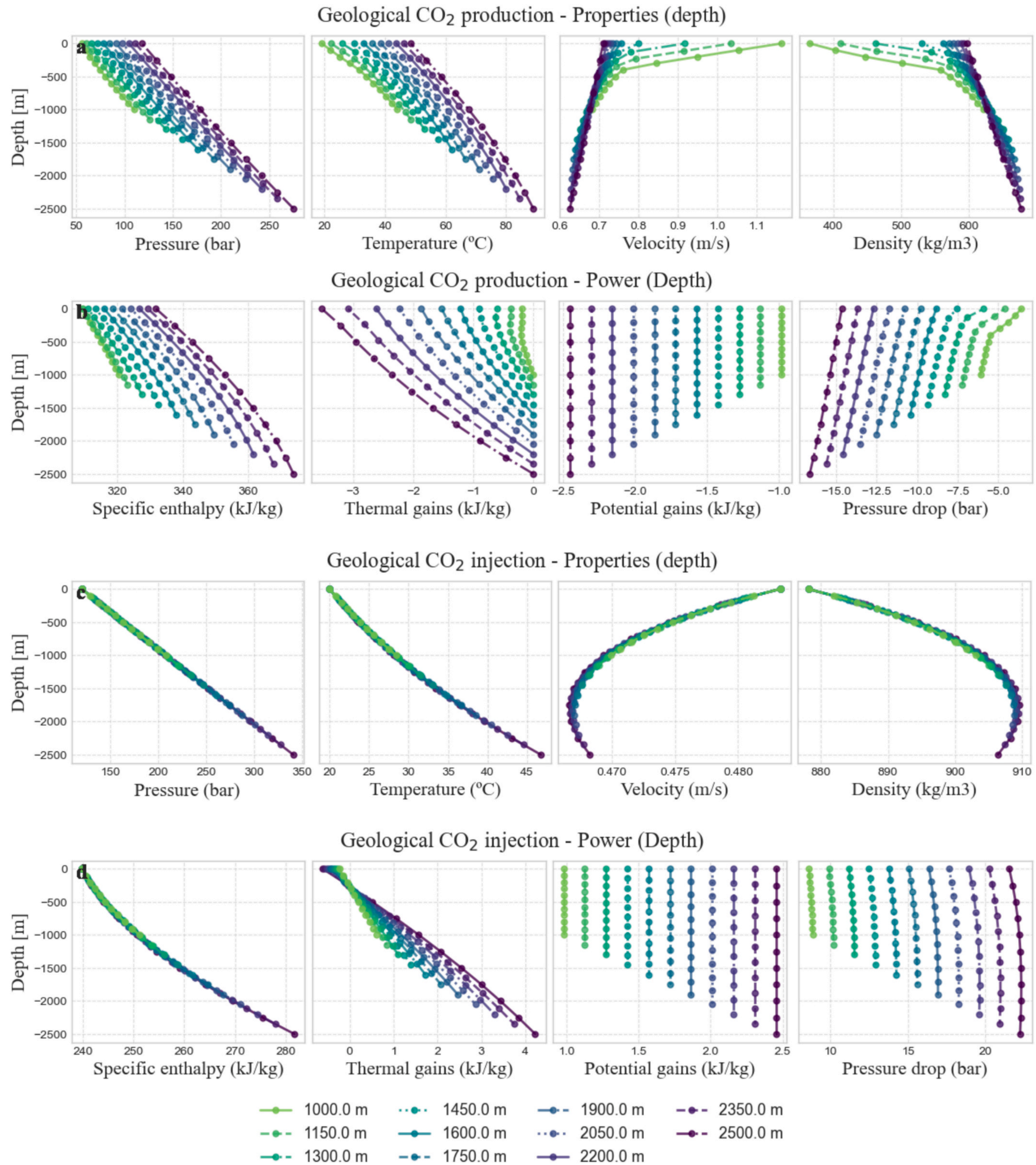

Fig. 8. CO_2 injection and production processes: a) Evolution of CO_2 properties (pressure, temperature, velocity and density) as a function of depth in the production process, b) Power gains (specific enthalpy, thermal gains, potential gains, pressure losses) as a function of depth in the production process, c) Evolution of CO_2 properties (pressure, temperature, velocity and density as a function of depth) as a function of depth in the injection process, d) Power gains (specific enthalpy, thermal gains, potential gains, pressure losses) as a function of depth in the injection process.

exceeded in cases where the previous dynamic steady state was close to this limit, as in the case of Fig. 7-right (injection mass flow rate higher than production and operational limitations in the injection process due to the upper pressure limit of the cavern). The model's ability to capture the damping effect of thermal mass in larger caverns (10,000 m^3 vs. 100 m^3) and the slow evolution toward geothermal equilibrium during shutdown periods matches the analytical solutions described in the foundational CAES stability studies [72].

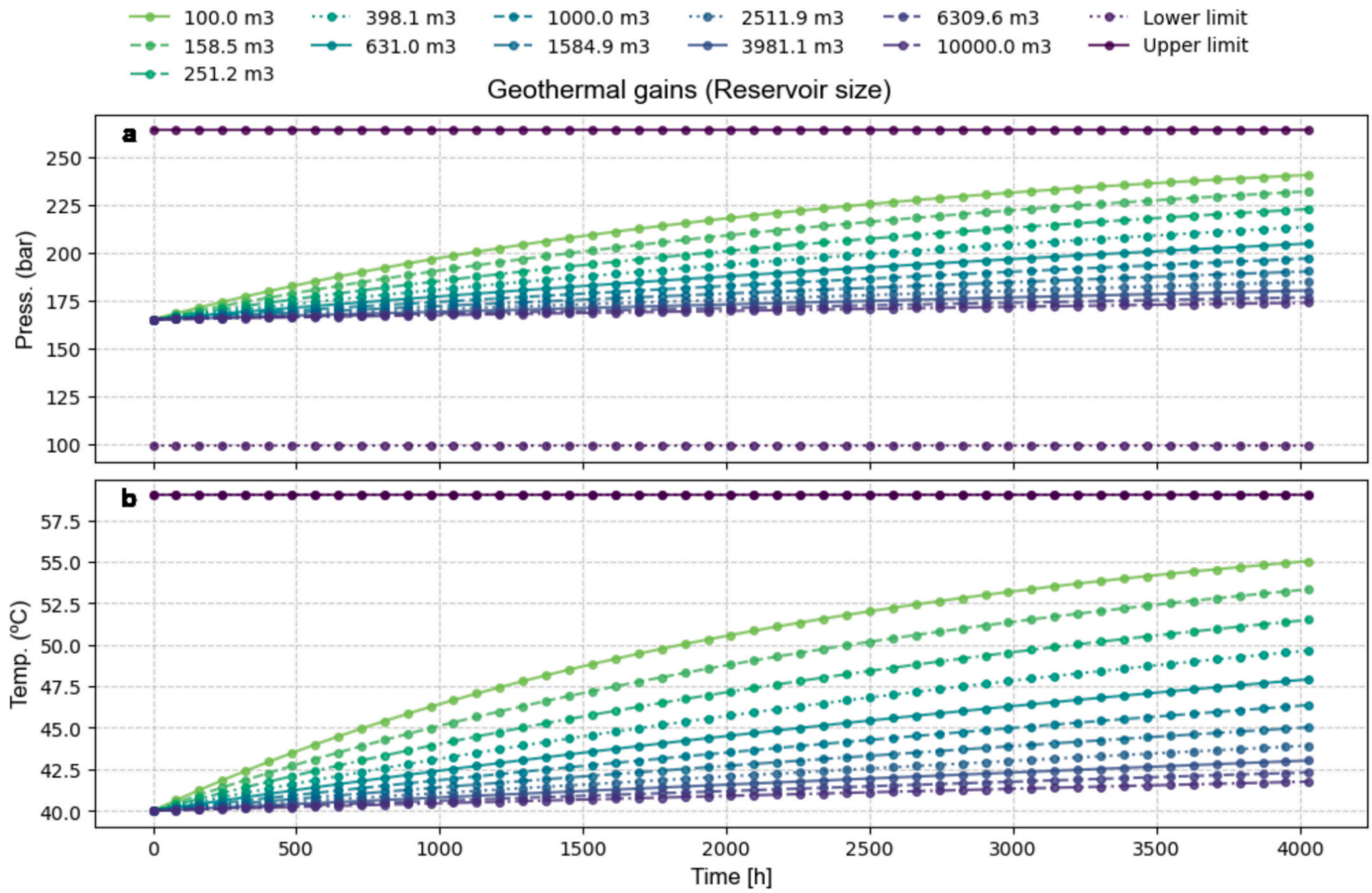

Fig. 9. Time evolution of the properties of CO_2 stored inside a salt cavity as a function of the volume of the salt cavity: a) time evolution of the pressure, b) time evolution of the temperature. Pressure limits are shown, set according to the lithostatic pressure of the cavern (30–80%) and the temperature of the geological formation (60 °C).

4. Conclusions

This study presents a system-level evaluation of a novel CO_2-based electrothermal energy and geological storage concept integrating transcritical CO_2 cycles with subsurface storage in salt caverns. The results indicate that the system is capable of achieving electric-to-electric efficiencies in the range of 52.8–61.5% under the assumed operating conditions. The thermodynamic performance is primarily governed by the surface cycles, while the subsurface system acts as a thermohydraulic buffer that constrains pressure and temperature conditions and enables long-term operational stability.

The saline cavity scenario involves pressure requirements within the geological formation, limited by lithostatic pressure, which is a function of depth. The surface thermal energy storage system involves alternating periods of injection, production, and shutdown. The salt cavity volume significantly influences the system's thermal dynamics. Smaller caverns experience faster increases in pressure and temperature, which benefits efficiency in short cycles, though it may limit operational stability. The CO_2 mass flow rates for injection and production depend on the plant's schedule and the size of the salt cavity. The criterion of using mass variations of 10% of the total CO_2 stored in the formation, at equilibrium conditions, is adequate to maintain the pressure within the limits. In a salt cavity of approximately 10,000 m^3, a mass flow rate of 30 kg/s is adequate using alternating operating periods of 6 h injection/production.

The salt cavern's energy balance is dominated by the injection and production streams, which depend on the wellhead conditions during injection, the mass flow ratio, and the operating period. The system evolves from an initial transient phase towards a state of thermodynamic stability after approximately 800–1000 h of operation. The new operating point must be selected, controlling the injection conditions, so that after production, it can be conditioned in terms of pressure and temperature to those required by the CO_2 transcritical cycle, in the dense liquid zone. Storage in the underground saline cavity under high-pressure (supercritical) conditions facilitates proper coupling between the surface and underground parts. This is a fundamental operational requirement for maintaining the shape of surface CO_2 transcritical cycles, operating with high conversion efficiency (>50%), surface thermal storage (7–10 MW_{th}) and incorporating mechanical energy storage (~500 kW). The analysis identifies a transition from an initial transient regime to a dynamic steady state after approximately 800–1000 h of operation, highlighting the importance of long-term simulations in assessing system behaviour.

The depth of the formation influences the conditions required at the injection wellhead to achieve the appropriate state within the saline formation during dynamic steady state. The behaviour of CO_2 during production and injection is governed by thermal and pressure gradients. During injection, pressure and temperature are increasing with depth, resulting in significant energy accumulation. The energy gain during injection directly influences the required CO_2 conditions at the wellhead. Wellhead pressure and temperature must be adjusted according to the desired conditions at the bottomhole. During production, fluid expansion causes a decrease in pressure, temperature, and density, and an increase in velocity. The production process may be interrupted if the properties of CO_2 at the wellhead evolve toward the gaseous zone, thereby limiting the plant's operating configuration.

The energy balance in the cavern is dominated by injection and production processes, while geothermal contributions remain secondary during cyclic operation but could become relevant during prolonged shut-in periods. The results further show that maintaining high-pressure conditions in the salt cavern is essential to ensure proper coupling with the surface cycles and to operate with high electricity-to-electricity conversion efficiencies, reaching the range of 50.3–65.6% when the pressure approaches the upper limit of this scenario. Suboptimal pressure regimes may lead to thermodynamic mismatches that reduce operational feasibility.

Geothermal heat transfer, whilst providing negligible geothermal heat transfer compared to the energy increases derived from injection and production processes, can have critical long-term effects. There is a risk of overpressure due to geothermal equilibrium during prolonged shut-in periods. Although thermal gains from the ground are minimal compared to those during cyclic operation phases, during extended closure periods, they become the sole driver of the energy balance, pushing the system towards a new steady state based on the ground temperature. This phenomenon causes a progressive increase in internal pressure, which, in high-capacity scenarios where the system is near its maximum threshold, may lead to an exceedance of cavern safety limits.

The modelling framework is based on a set of simplifying assumptions, including a lumped-parameter cavern model and one-dimensional wellbore representation. Therefore, the findings should be interpreted as first-order system-level trends, suitable for identifying design criteria and operational limits rather than detailed local phenomena. Overall, the proposed concept shows potential for large-scale energy storage applications, although further work is required to include more detailed geomechanical modelling, multi-dimensional effects, and experimental validation.

Regarding practical feasibility, the subsurface component is based on operational conditions and engineering approaches well established in industrial underground gas storage and CAES applications. The adopted pressure limits (30–80% lithostatic pressure), cavern depth range, and wellbore configurations are consistent with existing salt cavern storage practice and with previous studies on supercritical CO_2 storage in salt formations. Still, this is a first order system-level assessment rather than a site-specific engineering design. Future research should consider detailed analysis of operational constrains posed to wellbore management by batch injection and production of CO_2, and implications of the cavern geometry to the geothermal heat transfer and pressure build up during long closure periods.

Nevertheless, field deployment would require site-specific assessment of salt creep, cyclic thermo-mechanical loading, well integrity, sealing performance, and monitoring requirements. However, these aspects are routinely addressed for natural gas storage in salt caverns and do not represent fundamental technological barriers. In fact, the novelty of the approach does not lie on utilising the salt cavern for fluid storage itself, but on their integrated operation with surface thermal energy storage and transcritical CO_2 charge–discharge cycles.

These findings open new opportunities to design efficient and optimised hybrid energy storage systems that integrate flexible power generation with geological storage of captured CO_2, compatible with intermittent renewable sources such as PV, wind, and geothermal. Active management of mass flow rates and pressures, along with advanced thermal control strategies, will be essential to improve system efficiency and flexibility. The findings described in this study are critical for the proper design of the storage system, as they adequately couple the thermal energy storage and electrical power production cycle with underground CO_2 storage.

CRediT authorship contribution statement

A. Carro: Writing – original draft, Visualization, Validation, Software, Project administration, Methodology, Investigation, Funding acquisition, Formal analysis, Conceptualization. **J. Carneiro:** Writing – review & editing, Supervision, Methodology, Investigation, Funding acquisition, Conceptualization. **S. Unger:** Writing – review & editing, Investigation. **D. Behnous:** Writing – review & editing, Validation, Software. **S. Fogel:** Writing – review & editing, Investigation. **R. Chacartegui:** Writing – review & editing, Supervision, Project administration, Methodology, Investigation, Funding acquisition, Conceptualization.

Declaration of competing interest

The authors declare that they have no known competing financial interests or personal relationships that could have appeared to influence the work reported in this paper.

Acknowledgements

This work has been partially funded by the project 'CEEGS: Novel CO_2-based Electrothermal Energy and Geological Storage system', from the European Commission through Horizon, the EU Framework Programme for Research and Innovation, under Grant Agreement No. 101084376, and by a Juan de la Cierva fellowship, funded by the Spanish Ministry of Science, Innovation and Universities, the State Research Agency (MCIU/AEI/10.13039/501100011033) under grant JDC2024-055285-I, and the European Social Fund Plus (ESF+).

Data availability

Data will be made available on request.

References

[1] Aramendia E, Brockway PE, Taylor PG, Norman JB, Heun MK, Marshall Z. Estimation of useful-stage energy returns on investment for fossil fuels and implications for renewable energy systems. Nat Energy 2024;9:803–16. https://doi.org/10.1038/s41560-024-01518-6.
[2] Zhao J, Li F, Zhang Q. Impacts of renewable energy resources on the weather vulnerability of power systems. Nat Energy 2024. https://doi.org/10.1038/s41560-024-01652-1.
[3] Navia Simon D, Diaz Anadon L. Power price stability and the insurance value of renewable technologies. Nat Energy 2025. https://doi.org/10.1038/s41560-025-01704-0.
[4] van Heerden R, Edelenbosch OY, Daioglou V, Le Gallic T, Baptista LB, Di Bella A, et al. Demand-side strategies enable rapid and deep cuts in buildings and transport emissions to 2050. Nat Energy 2025. https://doi.org/10.1038/s41560-025-01703-1.
[5] Geth F, Brijs T, Kathan J, Driesen J, Belmans R. An overview of large-scale stationary electricity storage plants in Europe: current status and new developments. Renew Sustain Energy Rev 2015;52:1212–27. https://doi.org/10.1016/J.RSER.2015.07.145.
[6] Javed MS, Ma T, Jurasz J, Amin MY. Solar and wind power generation systems with pumped hydro storage: review and future perspectives. Renew Energy 2020;148:176–92. https://doi.org/10.1016/j.renene.2019.11.157.
[7] Zhang H, Baeyens J, Cáceres G, Degrève J, Lv Y. Thermal energy storage: recent developments and practical aspects. Prog Energy Combust Sci 2016;53:1–40. https://doi.org/10.1016/j.pecs.2015.10.003.
[8] Alva G, Lin Y, Fang G. An overview of thermal energy storage systems. Energy 2018;144:341–78. https://doi.org/10.1016/J.ENERGY.2017.12.037.
[9] Liang T, Vecchi A, Knobloch K, Sciacovelli A, Engelbrecht K, Li Y, et al. Key components for Carnot battery: technology review, technical barriers and selection criteria. Renew Sustain Energy Rev 2022;163:112478. https://doi.org/10.1016/J.RSER.2022.112478.
[10] Eppinger B, Zigan L, Karl J, Will S. Pumped thermal energy storage with heat pump-ORC-systems: comparison of latent and sensible thermal storages for various fluids. Appl Energy 2020;280:115940. https://doi.org/10.1016/j.apenergy.2020.115940.
[11] V. Novotny, V. Basta, P. Smola, J. Spale, Review of Carnot battery technology commercial development, Energies 2022, Vol. 15, Page 647 15 (2022) 647. Doi: 10.3390/EN15020647.
[12] Vecchi A, Knobloch K, Liang T, Kildahl H, Sciacovelli A, Engelbrecht K, et al. Carnot battery development: a review on system performance, applications and commercial state-of-the-art. J Energy Storage 2022;55:105782. https://doi.org/10.1016/J.EST.2022.105782.
[13] Paul A, Holy F, Textor M, Lechner S. High temperature sensible thermal energy storage as a crucial element of Carnot batteries: overall classification and technical review based on parameters and key figures. J Energy Storage 2022;56:106015. https://doi.org/10.1016/J.EST.2022.106015.
[14] C. Zhao, J. Yan, X. Tian, X. Xue, Y. Zhao, Progress in thermal energy storage technologies for achieving carbon neutrality, Carbon Neutrality 2023 2:1 2 (2023) 1–42. Doi: 10.1007/S43979-023-00050-Y.

[15] Li P, Yin H, Li H, Yang Y, Han Z. Thermo-economic performance assessment and multi-objective optimization of Carnot batteries with thermal integration. J Energy Storage 2025;125:117036. https://doi.org/10.1016/J.EST.2025.117036.

[16] Wang W, Xu S, Ju W, Shi L, Dai X. Optimization of Carnot battery systems under different decision criteria: configuration, working fluid and parameter. J Energy Storage 2025;125:116906. https://doi.org/10.1016/J.EST.2025.116906.

[17] Zhang C, Li M, Dang C, Chen X, Li X, Han Z. Enhanced Carnot battery for high-efficiency energy storage: feasibility analysis. Energy Convers Manag 2025;332: 119754. https://doi.org/10.1016/J.ENCONMAN.2025.119754.

[18] Liu Y, Wang Y, Huang D. Supercritical CO2 Brayton cycle: a state-of-the-art review. Energy 2019;189:115900. https://doi.org/10.1016/J.ENERGY.2019.115900.

[19] J. McTigue, P. Farres-Antunez, K. Ellingwood, T. Neises, A. White, Pumped thermal electricity storage with supercritical CO2 cycles and solar heat input, The VII International Young Researchers' Conference – Physics, Technology, Innovations (PTI-2020) 2313 (2020) 190024. Doi: 10.1063/5.0032337.

[20] V. Novotny, V. Basta, P. Smola, J. Spale, Review of Carnot battery technology commercial development, Energies 2022, Vol. 15, Page 647 15 (2022) 647. Doi: 10.3390/en15020647.

[21] Shamsi SSM, Barberis S, Maccarini S, Traverso A. Large scale energy storage systems based on carbon dioxide thermal cycles: a critical review. Renew Sustain Energy Rev 2024;192. https://doi.org/10.1016/j.rser.2023.114245.

[22] Tang J, Li Q, Wang L, Yu H. Process integration of supercritical CO2 cycle and pumped thermal energy storage (PTES) system. Chem Eng Trans 2024;114:13–8. https://doi.org/10.3303/CET24114003.

[23] Girelli S, Morosini E, Alfani D, Astolfi M. Design and techno-economic assessment of a transcritical CO2 pumped thermal energy storage system. Energy 2025;339. https://doi.org/10.1016/j.energy.2025.138902.

[24] Liang Z, Chen P, Lu P, Luo X, Liang Y, Chen J, et al. Thermo-economic analysis and evaluation of a novel super/trans-critical CO2 Carnot battery based on partial condensation and recompression. Renew Energy 2026;256. https://doi.org/10.1016/j.renene.2025.124543.

[25] Chang T, Song Y, Li S, Zhang Y, Cui C, Cao F. Energetic investigation on the dynamic operation characteristics of distributed Carnot Batteries with high temperature transcritical CO2 heat pump. J Energy Storage 2026;147:120108. https://doi.org/10.1016/j.est.2025.120108.

[26] Mercangöz M, Hemrle J, Kaufmann L, Z'Graggen A, Ohler C. Electrothermal energy storage with transcritical CO2 cycles. Energy 2012;45:407–15. https://doi.org/10.1016/j.energy.2012.03.013.

[27] Liu X, Wang D, Peng X, Wang G, Yang Y. Experimental study on performance and compressor characteristics of transcritical CO2 heat pump system. Appl Therm Eng 2024;250:123524. https://doi.org/10.1016/J.APPLTHERMALENG.2024.123524.

[28] S. Guccione, S. Trevisan, R. Guedez, Optimum coupling of thermal energy storage and power cycles, Proceedings of the ASME Turbo Expo 6 (2023). Doi: 10.1115/GT2023-103939.

[29] S. Unger, S. Fogel, P. Schütz, R. Chacartegui Ramirez, A. Carro, J. Carneiro, U. Hampel, The sCO2 Facility CARBOSOLA: design, purpose and use for investigating geological energy storage cycles, in: Proceedings of the ASME Turbo Expo 2024: Turbomachinery Technical Conference and Exposition. Volume 11: Supercritical CO2. London, United Kingdom. June 24–28, 2024. V011T28A004. ASME, American Society of Mechanical Engineers Digital Collection, 2024. Doi: 10.1115/GT2024-122133.

[30] Carro A, Chacartegui R, Ortiz C, Carneiro J, Becerra JA. Energy Storage System based on transcritical CO2 cycles and geological storage. Appl Therm Eng 2021; 193:116813. https://doi.org/10.1016/j.applthermaleng.2021.116813.

[31] Carro A, Chacartegui R, Ortiz C, Carneiro J, Becerra JA. Integration of energy storage systems based on transcritical CO2: Concept of CO2 based electrothermal energy and geological storage. Energy 2022;238:121665. https://doi.org/10.1016/J.ENERGY.2021.121665.

[32] Carneiro JF, Matos CR, van Gessel S. Opportunities for large-scale energy storage in geological formations in mainland Portugal. Renew Sustain Energy Rev 2019;99: 201–11. https://doi.org/10.1016/j.rser.2018.09.036.

[33] Behnous D, Carneiro J, Carro A, Canteli P, Chacartegui R, Crespo JG, et al. Optimising supercritical CO2 saturation and reservoir conditions for geological energy storage with transcritical carbon dioxide systems. J Energy Storage 2025; 139:118924. https://doi.org/10.1016/J.EST.2025.118924.

[34] Carro A, Carneiro J, Ortiz C, Behnous D, Becerra JA, Chacartegui R. Assessment of carbon dioxide transcritical cycles for electrothermal energy storage with geological storage in salt cavities. Appl Therm Eng 2024;255:124028. https://doi.org/10.1016/J.APPLTHERMALENG.2024.124028.

[35] J. Carneiro, D. Behnous, A. Carro, P. Canteli, R. Chacarteugui, J.G. Crespo, M.P. Farkas, E. Gianni, N. Koukouzas, C. Schmidt-Hattenberger, P. Tyrologou, A.-S. Kyriakides, A. Stoikos, D. Trigkas, G. Gravanis, I.N. Tsimpanogiannis, S. Voutetakis, Geological scenarios and constraints for the implementation of the CO2-based Electrothermal Energy and Geological Storage System (CEEGS) concept, 17th International Conference on Greenhouse Gas Control Technologies GHGT-17 (Calgary, Canada 2024). (2024).

[36] CEEGS Project, Novel CO2-based electrothermal energy and geological storage system, (n.d.). https://ceegsproject.eu/ (accessed March 18, 2024).

[37] Carro A, Ortiz C, Unger S, Stoikos A, Kyriakides AS, Tsimpanogiannis IN, et al. Surface processes optimisation in a novel CO2-based electrothermal energy and geological storage trigeneration system. Appl Energy 2025;395:126165. https://doi.org/10.1016/J.APENERGY.2025.126165.

[38] S. Unger, S. Fogel, P. Schütz, R. Chacartegui, A. Carro, M.P. Farkas, C. Schmidt-Hattenberger, U. Hampel, Experimental investigation of the power production cycle in a CO2 based electrothermal energy and geological storage system, in: 6th Edition of the European Conference on Supercritical CO2 (SCO2) for Energy Systems: April 09–11, 2025, Delft, The Netherlands, DuEPublico - Duisburg-Essen Publications Online, 2025: pp. 306–314. Doi: 10.17185/DUEPUBLICO/83305.

[39] Okolie JA, Nanda S, Dalai AK, Kozinski JA. Advances in the industrial applications of supercritical carbon dioxide. Carbon Dioxide Capture and Conversion: Advanced Materials and Processes 2022:237–56. https://doi.org/10.1016/B978-0-323-85585-3.00008-0.

[40] Bangalore Mohankumar M, Unger S, Guille A, Carro A, Chacartegui Ramírez R, Hampel U. Thermal performance assessment of high-temperature sensible solid thermal energy storage (SSTES): various designs. Storage Materials and Heat Transfer Fluids 2024. https://doi.org/10.1115/GT2024-126448.

[41] Li W, Yu Z. Heat exchangers for cooling supercritical carbon dioxide and heat transfer enhancement: a review and assessment. Energy Rep 2021;7:4085–105. https://doi.org/10.1016/J.EGYR.2021.06.089.

[42] Ma Y, Xie G, Hooman K. Review of printed circuit heat exchangers and its applications in solar thermal energy. Renew Sustain Energy Rev 2022;155:111933. https://doi.org/10.1016/J.RSER.2021.111933.

[43] Lugo A, Turunen-Saaresti T, Tiainen J. Effects of supercritical CO2 fluid properties on heat exchanger design. Proc ASME Turbo Expo 2023;12. https://doi.org/10.1115/GT2023-101612.

[44] Ma Y, Liu D, Wang J, Zeng M, Wang Q, Ma T. Thermal-hydraulic performance and optimization of printed circuit heat exchangers for supercritical fluids: a review. Renew Sustain Energy Rev 2025;208:115051. https://doi.org/10.1016/J.RSER.2024.115051.

[45] Wang Z, Wang D, Ren X, Xue M, Wang T, Wan M, et al. A review of supercritical carbon dioxide heat transfer and flow properties in pipes. Energ Technol 2025;13: 2401461. https://doi.org/10.1002/ENTE.202401461;PAGE:STRING:ARTICLE/CHAPTER.

[46] Guisado JM, Carro A, Unger S, Kyriakides AS, Tsimpanogiannis IN, Hampel U, et al. Analytical investigation of the compressor layout for off-design operation of a transcritical CO2 cycle in an electrothermal energy storage. Energy Convers Manage: X 2025;28:101299. https://doi.org/10.1016/J.ECMX.2025.101299.

[47] Toni L, Bisio V, Milani A, Biliotti D, Bellobuono E, Valente R, et al. Supercritical CO2 compressor and expander design for industrial waste-heat valorization. Proc ASME Turbo Expo 2023;12. https://doi.org/10.1115/GT2023-102558.

[48] Jiang P, Wang B, Tian Y, Xu X, Zhao L. Design of a supercritical CO2 compressor for use in a 1 MWe power cycle. ACS Omega 2021;6:33769–78. https://doi.org/10.1021/ACSOMEGA.1C05023/ASSET/IMAGES/LARGE/AO1C05023_0016.JPEG.

[49] Liu K, Guo Y, Wang L, Fan G, Che D. Control of supercritical CO2 Brayton cycle for fast and efficient load variation processes. Appl Therm Eng 2024;244:122797. https://doi.org/10.1016/J.APPLTHERMALENG.2024.122797.

[50] A. Carro, J. Carneiro, S. Unger, P. Mesquita, S. Fogel, R. Chacartegui, CO2 transport and geological storage under supercritical conditions: preliminary study of the integration with renewable electrothermal energy storage, in: 6th Edition of the European Conference on Supercritical CO2 (SCO2) for Energy Systems: April 09–11, 2025, Delft, The Netherlands, DuEPublico - Duisburg-Essen Publications Online, 2025: pp. 232–243. Doi: 10.17185/DUEPUBLICO/83271.

[51] White MT, Bianchi G, Chai L, Tassou SA, Sayma AI. Review of supercritical CO2 technologies and systems for power generation. Appl Therm Eng 2021;185: 116447. https://doi.org/10.1016/J.APPLTHERMALENG.2020.116447.

[52] S.D. Cich, K. Hoopes, J.J. Moore, J. Mortzheim, M. Marshall, D. Hofer, Radial inlet and exit design for a 10 MWe sCO2 axial turbine, Proceedings of the ASME Turbo Expo 9 (2019). Doi: 10.1115/GT2019-90392.

[53] Lee S, Gurgenci H. A comparison of three methodological approaches for meanline design of supercritical CO2 radial inflow turbines. Energy Convers Manag 2020; 206:112500. https://doi.org/10.1016/J.ENCONMAN.2020.112500.

[54] Allison TC, Moore J, Pelton R, Wilkes J, Ertas B. Turbomachinery, fundamentals and applications of supercritical carbon dioxide (SCO2). Based Power Cycles 2017: 147–215. https://doi.org/10.1016/B978-0-08-100804-1.00007-4.

[55] Pourahmadiyan A, Sadi M, Arabkoohsar A. Seasonal thermal energy storage, future grid-scale energy storage solutions: mechanical and chemical technologies and principles. 2023, 215–267. Doi: 10.1016/B978-0-323-90786-6.00013-3.

[56] Kalaiselvam S, Parameshwaran R. Latent thermal energy storage. Thermal Energy Storage Technologies for Sustainability 2014:83–126. https://doi.org/10.1016/B978-0-12-417291-3.00005-0.

[57] Yan J, Zhang X. Application and development of dynamic ice slurry technology. In: 2010 International Conference on Mechanic Automation and Control Engineering; 2010. p. 1441–4. https://doi.org/10.1109/MACE.2010.5536141.

[58] Rayhan FA, Yanuar ASP. Effect of ice mass fraction on ice slurry flow for cold energy storage application. Energy Reports, Elsevier Ltd 2020:790–4. https://doi.org/10.1016/j.egyr.2019.11.159.

[59] Liu W, Zhang X, Wan J, Yang C, Jiang L, Chen Z, et al. Large-scale carbon dioxide storage in salt caverns: evaluation of operation, safety, and potential in China. Engineering 2024;40:226–46. https://doi.org/10.1016/J.ENG.2024.06.013.

[60] Minkley W, Brandt M, Dostal V, Stepanek J. Energy storage in salt caverns with supercritical CO2. The Mechanical Behavior of Salt X 2022:639–51. https://doi.org/10.1201/9781003295808-58.

[61] Mwakipunda GC, Mgimba MM, Ngata MR, Yu L. Recent advances on carbon dioxide sequestration potentiality in salt caverns: a review. Int J Greenhouse Gas Control 2024;133:104109. https://doi.org/10.1016/J.IJGGC.2024.104109.

[62] Khaledi K, Mahmoudi E, Datcheva M, Schanz T. Stability and serviceability of underground energy storage caverns in rock salt subjected to mechanical cyclic loading. Int J Rock Mech Min Sci 2016;86:115–31. https://doi.org/10.1016/J.IJRMMS.2016.04.010.

[63] Liu X, Wang J, Wang X, Lin Y, Liu X, Song Z. Fatigue properties and damage evolution of salt rock after thermal cycling treatment. Rock Mech Rock Eng 2025; 2025:1–23. https://doi.org/10.1007/s00603-025-05026-1.

[64] Liao Y, Wang T, Li L, Ren Z, Xie D, He T. Thermal analysis for gas storage in salt cavern based on an improved heat transfer model. Appl Therm Eng 2023;232:121112. https://doi.org/10.1016/j.applthermaleng.2023.121112.

[65] Li W, Nan X, Chen J, Yang C. Investigation of thermal-mechanical effects on salt cavern during cycling loading. Energy 2021;232:120969. https://doi.org/10.1016/j.energy.2021.120969.

[66] Bell IH, Wronski J, Quoilin S, Lemort V. Pure and pseudo-pure fluid thermophysical property evaluation and the open-source thermophysical property library coolprop. Ind Eng Chem Res 2014;53:2498–508. https://doi.org/10.1021/IE4033999/SUPPL_FILE/IE4033999_SI_002.ZIP.

[67] Morandin M, Maréchal F, Mercangöz M, Buchter F. Conceptual design of a thermo-electrical energy storage system based on heat integration of thermodynamic cycles - part A: Methodology and base case. Energy 2012;45:375–85. https://doi.org/10.1016/j.energy.2012.03.031.

[68] Morandin M, Maréchal F, Mercangöz M, Buchter F. Conceptual design of a thermo-electrical energy storage system based on heat integration of thermodynamic cycles – part B: alternative system configurations. Energy 2012;45:386–96. https://doi.org/10.1016/J.ENERGY.2012.03.033.

[69] Adams BM, Kuehn TH, Bielicki JM, Randolph JB, Saar MO. On the importance of the thermosiphon effect in CPG (CO2 plume geothermal) power systems. Energy 2014;69:409–18. https://doi.org/10.1016/j.energy.2014.03.032.

[70] Li X, Li G, Wang H, Tian S, Song X, Lu P, et al. A unified model for wellbore flow and heat transfer in pure CO2 injection for geological sequestration, EOR and fracturing operations. Int J Greenhouse Gas Control 2017;57:102–15. https://doi.org/10.1016/J.IJGGC.2016.11.030.

[71] Soubeyran A, Rouabhi A, Coquelet C. Thermodynamic analysis of carbon dioxide storage in salt caverns to improve the Power-to-Gas process. Appl Energy 2019;242:1090–107. https://doi.org/10.1016/J.APENERGY.2019.03.102.

[72] Allen RD, Doherty TJ, Thoms RL. Geotechnical factors and guidelines for storage of compressed air in solution-mined salt cavities, 1982. Doi: 10.2172/5234728.